EMBEDDING ANTENNA SHEAR/PRESSURE SENSORS IN PROSTHETIC LINER MATERIAL

by

SHAHNAVAZ EILBEIGI

Presented to the Faculty of the Graduate School of

The University of Texas at Arlington in Partial Fulfillment

of the Requirements

for the Degree of

MASTER OF SCIENCE IN MECHANICAL ENGINEERING

THE UNIVERSITY OF TEXAS AT ARLINGTON

August 2016

Acknowledgements

I greatly appreciate my advisor, Prof. Huang for her help, patience and support, and also for trusting me by giving me the opportunity to prove myself and be part of Advanced Sensor Technology Laboratory. It has certainly been a rewarding experience to work with her. I am also thankful to her for providing financial assistance during the two years of my graduate study.

Of course, I need to give special thanks to my father Malek Hossein, my mother Parivash, my brother Salar, my grandmother Iran and my aunt Parvane, who are the only reason for me being here, and for all of their love and support.

I would like to extend my thanks to all my lab-mates and my friends especially Behzad Zamanian for training me advanced SolidWorks.

Last but not least, I thank UTA for giving me the opportunity to continue my education as a Master of Science student, which has allowed me to grow personally and professionally.

May 3, 2016

Abstract

EMBEDDING ANTENNA SHEAR/PRESSURE SENSORS

IN PROSTHETIC LINER MATERIAL

SHAHNAVAZ EILBEIGI, M.S

The University of Texas at Arlington, 2016

Supervising Professor: Haiying Huang

Published surveys indicated that 40-60% of prosthesis users experience discomfort and skin problems. These studies highlighted the needs for enhanced prosthetic performance and fit. It is extremely difficult to address these problems due to two reasons: first, ambulation create varying areas of shear and pressure on the residual limb, but it is not clear which shear/ pressure combinations are acceptable and what is the safe stress level for users. In addition, the volume of the residual limb changes throughout the day and activity level. Therefore, there is a strong need to develop a light, thin, flexible, and wirelessly interrogated sensor for an in-socket system that can measure the interface stresses at real-time. Our team presented a microstrip patch antenna sensor that is capable to measure the shear and normal deformations simultaneously. According to the principle of multi-layer microstrip patch antenna, the shear/pressure antenna sensor consists of a microstrip patch antenna and a U-shaped reflector separated by a layer of liner material. In this thesis, detailed investigations on the design of proposed sensor are presented and simulated using numerical simulation software. Different fabrication techniques are developed to fabricate the microstrip patch antenna and the reflector on thin flexible substrates, to integrate shear/pressure antenna sensor with commercial prosthetic liner, and to embed it in custom-made liners. The material

selection criteria, the characterization of material properties, and the challenges facing the fabrication techniques are described in details. The radiation characteristics of fabricated sensors with/without liner were measured experimentally and compared with the simulation results to validate the sensor design. A method to design and fabricate antenna sensors with long transmission line also is presented and simulated. Finally, for characterizing the antenna sensors on an able-bodied volunteer, two different fabrication techniques are developed to embed two long antenna sensors in real-size custom-made prosthetic liner. In this thesis, some novel approach also are presented like: 1- Designed and validated complete fabric antenna sensor to improve the flexibility and compatibility; 2- Designed and validated the patch antenna with a meandering transmission line; which future work will provide the embedding and characterizing of such sensors in the custom-made prosthetic liner.

Table of Contents

Acknowledgements i

Abstract ii

Table of Contents iv

List of Illustrations vii

List of Tables xi

Chapter 1 INTRODUCTION 1

1.1 History of Prosthesis 1

1.2 Sockets and Prosthetic Liners 2

1.3 Prosthetics Fitting 3

1.4 Skin Problems 4

1.5 Current Shear and Pressure Sensors 5

1.5.1 Strain-gauge 6

1.5.2 Piezoresistive 7

1.5.3 Capacitive 7

1.5.4 Fiber Optic 8

1.6 Different Sensors Mounting and Fabrication Techniques 8

1.7 Proposed Shear and Pressure Sensors and Fabrication Technique 10

1.8 Advantageous of the Proposed Antenna Sensing Prosthetic Liner 11

1.9 Thesis Indexing 11

Chapter 2 MICROSTRIP PATCH ANTENNA FUNDAMENTALS 13

2.1 History 13

2.2 Basics of the Microstrip Patch Antenna 15

2.3 Feeding Methods 16

2.3.1 Microstrip line 18

2.4 Microstrip Patch Antenna Analysis 18
2.4.1 Transmission Line Model 18
2.5 Shear and Pressure Antenna Sensor 19
2.5.1 Patch Antenna as Shear and Pressure Sensor 21
Chapter 3 SENSOR DESIGN AND SIMULATION 23
3.1 Design of Rectangular Microstrip Patch Antenna 23
3.2 Design of Microstrip Patch Antenna with Superstrate 28
Chapter 4 SENSOR FABRICATION 35
4.1 Microstrip Patch Antenna Fabrication 35
4.1.1 Fabricate Antenna Sensor from Kapton/Copper Films using Vacuum Lamination 35
4.1.2 Fabricate Patch Antenna from Flexible Printed Circuit Boards 40
4.2 Material Selection and Characterization 42
4.2.1 Commercial Prosthetic Liner Material 42
4.2.2 Integrating the shear and pressure sensor in commercial prosthetic liner 43
4.2.3 Custom-made liner material 47
Chapter 5 IMPLEMENTING ANTENNA SENSORS IN CUSTOM-MADE LINER 56
5.1 Long Transmission Line Antenna Design 56
5.1.1 Quarter-wave length method 56
5.2 Long Antenna Transmission Line Fabrication and Measurement 60
5.2.1 SMA Connector Stabilization 63
5.3 Final Implementation of long transmission line antenna sensors in custom-made liner 65

5.3.1 First Technique: Casting the liner using a real-size mold 65
5.3.2 Second Technique: Casting the liner in sheet form 67
Chapter 6 ANTENNA SENSOR ENHANCEMENT 69
6.1 Electrode Material 69
6.1.1 Flexible Conductive Foam/ Fabric Antenna Sensors 70
6.2 Dielectric Substrate Material 73
6.2.1 Mature fabric antenna sensor 74
6.3 Meandering transmission line 75
6.3.1 Design and Simulation of Meandered line Patch Antenna 76
6.3.2 Validation of Meandered line patch antenna 79
Chapter 7 CONCLUSION 81
Chapter 8 FUTURE WORKS 83
Appendix A Material Data Sheet 85
Appendix B SolidWorks Layout 92
Biographical Information 101

List of Illustrations

Figure 2-1 Microstrip patch antenna; (a) schematic diagram of microstrip patch antenna; (b) typical shapes of microstrip patch antenna 15

Figure 2-2 Schematic of rectangular microstrip patch antenna 16

Figure 2-3 3-D view of microstrip antenna feeding methods; (a) microstrip line; (b) coaxial line; (c) aperture coupled feed; (d) proximity coupled feed [51] 17

Figure 2-4 Electric field lines in transmission line 19

Figure 2-5 Fringing field for the dominant mode in a rectangular microstrip patch antenna 19

Figure 2-6 Multi-layer shear and pressure sensor 21

Figure 2-7 Lateral displacement between patch antenna and reflector due to shear deformation 21

Figure 2-8 Vertical displacement between patch antenna and reflector due to compression 22

Figure 3-1 Typical design procedures for rectangular patch antenna 27

Figure 3-2 Microstrip patch antenna; (a) simulation model of a patch antenna; 28

Figure 3-3 Side view configuration of a microstrip patch antenna covered with superstrate 29

Figure 3-4 Conformal mapping process of a multidielectric rectangular microstrip patch antenna 30

Figure 3-5 Design of patch antenna sensor and reflector (All dimensions are in mm) 33

Figure 3-6 Microstrip patch antenna with superstrate; (a) simulation model of a patch antenna; (b) simulated radiation characteristics of proposed patch antenna 34

Figure 4-1 Basic of vacuum bagging assembly 36

Figure 4-2 Fabrication steps of the patch antenna using vacuum lamination 39

Figure 4-3 $S11$ parameter of the fabricated microstrip patch antenna using vacuum lamination technique 40
Figure 4-4 Microstrip patch antenna; (a) final photo-etched fabricated microstrip patch antenna and reflector; (b) comparison between measured and simulated radiation characteristics of fabricated microstrip patch antenna..... 42
Figure 4-5 Shear and pressure antenna sensor bonded on commercial prosthetic liner . 45
Figure 4-6 Comparison between the measured and simulated scattering parameters of shear/pressure antenna sensor bonded on commercial prosthetic liner 46
Figure 4-7 Flow chart of different classes of silicone material 48
Figure 4-8 Test fixture for shear and pressure tests of soft silicone materials 50
Figure 4-9 Characterizes the compression and shear moduli of silicone materials; 52
Figure 4-10 Shear and pressure antenna sensor implemented with soft liner materials as superstrate; (a) embedding Flexible patch antennas in 5 mm thick RTV silicone material using the flat mold; (b) flexible patch antenna embedded in 7 mm thick RTV silicone rubber 55
Figure 5-1 Microstrip patch antenna using quarter wavelength transformer 57
Figure 5-2 Model of long transmission line patch antenna; edge-fed with two quarter-wavelength transformer..... 58
Figure 5-3 Antenna sensors with a long transmission line; (a) numerical simulation model of shear/pressure antenna sensor with two quarter-wavelength transformers;..... 60
Figure 5-4 Long rectangular patch antenna; (a) patch antenna and transmission line fabricated on soft substrate; (b) comparison between measured and simulated $S11$ parameters 61

Figure 5-5 Characterization of the antenna sensor with a long transmission line; (a) $S11$ signal represented in time-domain; (b) Spectrum of time-gated signal; (c) Filtered $S11$ signal 62
Figure 5-6 Antenna sensor and SMA connector fixture; (a) first configuration; (b) second configuration 64
Figure 5-7 Embed antenna sensors in custom-made prosthetic liner (first technique); ... 66
Figure 5-8 Fabricated prosthetic liner with embedded antenna sensors (first technique) 67
Figure 5-9 Embed antenna sensors in custom-made prosthetic liner (Second technique); (a) fabrication the liner in sheet form; (b) trimming and forming of the liner using Velcro straps 68
Figure 6-1 Implementing flexible sensor using conductive foam/fabric; (a) conductive foam antenna and reflector bonded on Kapton film; (b) conductive foam antenna and reflector bonded on PTFE film; (c) flexibility of antenna fabricated from conductive foam; (d) conductive fabric antenna; (e) flexibility of antenna fabricated from conductive fabric 71
Figure 6-2 Comparison between the measured $S11$ curves of fabricated sensors; (conductive foam patch antenna based on Kapton substrate (Green-line); conductive foam patch antenna based on PTFE substrate (Red-line) and conductive fabric patch antenna based on PTFE substrate (Blue-line)) 72
Figure 6-3 Complete fabric-based antenna sensor; (a) fabricated antenna sensor; (b) $S11$ parameter of the fabric-based antenna sensor 75
Figure 6-4 Patch antenna with meandering transmission line dimensions 76
Figure 6-5 Three different configurations for mitered corners; (a) regular mitered corner; (b) improved mitered corner; (c) large mitered corner 78

Figure 6-6 Antenna sensors with meandering transmission lines; (a) numerical simulation model of patch antenna with meandering transmission lines ;(b) Simulated radiation characteristics of proposed meandering antenna 79
Figure 6-7 Meandered line patch antenna; (a) fabricated patch antennas with meandering transmission lines having two different bending types; (b) comparison between the measured and simulated $S11$ parameters of an antenna sensor with a mitered meandering transmission line 80
Figure 8-1 Final prototype of fabricated liner with antenna sensors; (a) the liner wore by a volunteer; (b) the liner inside a socket wore by a volunteer. 83
Figure 8-2 S11 parameter collected from the sensor embedded in the custom-made liner at different fitness of the socket 84

List of Tables

Table 3-1 Properties of RO3003 Laminate 26

Table 4-1 Used vacuum bagging equipment [64] 36

Table 4-2 Advantage and disadvantage of the used elastic material for liners [66] 42

Table 4-3 Comparison of the available samples from different companies [67] 43

Table 4-4 Selected silicone materials for custom-made prosthetic liner (Appendix A.3) . 50

Table 5-1 Designed parameter of long microstrip patch antenna 59

Chapter 1

INTRODUCTION

1.1 History of Prosthesis

An artificial limb or prosthesis is defined as a device that intends to replace the failure of a limb either with the functional or cosmetic attraction for the amputee [1]. The evolution and development of prosthetics is a long and storied history, starting from its ancient beginnings to its complicated present, to the exhilarating visualizations of the upcoming [2]. As with the advancements of some other fields, several inventions and ideas have been employed and extended upon, for example, the foot with fixed-position, whereas others have plunged by the edge or become superseded, just like the utilization of iron in prosthesis [3]. In 2000, investigators in Egypt revealed what they purported to be the most ancient artificial part of the body, an artificial toe formed of leather and wood [4].

The extended and meandering road to the automated leg initiated about 1500 B.C. and has been developing ever since. Egyptians were considered to be early on pioneers of synthetic and prosthetic technology. Their basic prosthetic limbs were made by using fiber. Dating about 300 B.C. a synthetic leg was discovered in Italy in 1858. It was formed by using a combination of iron and bronze with a wooden core, and was utilized for the amputee below the knee [5]. In 424 B.C., an historian wrote about a Persian clairvoyant who was sentenced to death but escaped with the help of amputating his foot and creating a stilted filler to saunter 30 miles to a nearby town.

The Dark Ages observed slight development in the field of prosthetics except for the peg leg. Most of the prostheses of that time were produced to hide injuries and deformities as a result of battle [6]. It was very common for the tradesmen, which included the armorers, to devise, create and design artificial limbs [7]. Different

tradesmen contributed greatly in the formation of devices, particularly the watchmakers, who were instrumental in the addition of complex interior functions with gears and springs [8].

The medical inventions of the Romans and Greeks represented a revival in prosthetics history. During this period, the prostheses were commonly formed of iron, wood, steel and copper [3].

The French Army surgeon, Ambroise Paré, is considered as the father of current prosthetic design and amputation surgery. In 1529, he initiated the procedures of modern amputation to the community of medicine, and formed prostheses (1536) for lower and upper extremity amputees [9]. He also discovered a device – a foot prosthesis and a kneeling peg leg - that had an adjustable harness, fixed position, and control of the knee lock and other features of engineering used in present day devices. His discoveries revealed the first accurate consideration of the functioning of prosthesis. A French locksmith, Lorrain, (colleague of Paré's) presented the most significant contributions in the field, while utilizing glue, paper and leather instead of iron in the production of a prosthesis [3, 10].

In 1969, Pieter Verduyn invented the first prosthesis, known as the non-locking below-knee prosthesis, that later develop into the outline for current corset devices and joints [11].

1.2 Sockets and Prosthetic Liners

A prosthesis is made up of two main parts: the exterior socket and an interior liner. The socket is defined as the outer hard portion formed with the residual limb of the individual. It is also known as that part of the prosthesis which holds the stump of amputation. The purpose of hard socket is to maintain the residual limb and perform as

an edge for the forged limb, either for a prosthetic leg, foot or arm. The interior liner acts as an edge connecting the hard socket with the residual limb and is made up of a soft silicone-like material. The sockets are of different types, including adjustable sockets, air-cushion sockets, diagonal sockets, Dundee sockets, hard sockets, partial-contact sockets, plug fit sockets, quadrilateral sockets, rigid sockets, segmental sockets, semi-rigid sockets, slip sockets, soft sockets, split sockets, suction sockets and the total-contact socket. These sockets are made of different materials and serve different purposes as well [12].

1.3 Prosthetics Fitting

The investigators have been interested in measuring the interference stresses so as to estimate the amount of any probable harm caused as a result of the contact between the hard socket and the tissues of the residual limb [13]. In recent years, several measurement techniques have been engaged in an attempt to: (1) recognize points of extreme stress which might lead to a breakdown of the skin (2) determine distribution of stress in various socket designs, and (3) assess suspension systems and cushioning of interface amongst others [14, 15]. The results of such techniques of measurement have contributed in the improvement of design and appropriate fitting of transtibial hard sockets. The purpose of this literature review is to assess the operating benefits, disadvantages and principles of emerging, conventional techniques which are used for interfacing the stress measurements present inside the transtibial hard sockets, give important and valuable insights into the recent trends in fitting the socket and the critical considerations for an effectual tools of measurement at real time that can direct us to a purposeful prosthetic socket.

To guarantee the correct force distribution, the socket should maintain an intimate fitting with the residual limb. It should offer a natural feel and allocate the forces all through the limb [16]. Volume stabilization is important for the residual limb in order to feel comfort, reduce breakdown of tissue, and develop daily activity. In a current study, the volumes of the residual limb fluctuated by 6.5% within a 24 hour time period [17]. Loss of volume of the residual limb can result in loosening, inappropriate allotment of forces bearing mass and weight and improper fitting of the limb in the hard socket. This can result in shear force and increased pressure on the residual limb that can lead to breakdown of the skin and reduced control and power on the prosthesis [18].

1.4 Skin Problems

The shear and pressure combination on the socket and the liner interface differ among individuals, sites and clinical circumstances. Still, the type of design does not matter. It is always vital to feature in the pattern of transfer of load. This will be helpful for the designers in assessing the fitting quality and will improve their understanding and knowledge of the fundamental biomechanical basis [19]. The distribution of pressure and shear between the socket and the limb is an important concern when it approaches the design and fit of the socket. It is important to recognize the response of the tissues of the residual limb to the exterior loads and other outer phenomenon at this point [20].

The generated localized stresses are of two types, those generated within a prosthetic socket and those generated on the residual limb during the process of ambulation. One is the normal stresses (which are perpendicular to interface) and the other is the shear stresses (in the interface plane). Both of these shear and normal stresses are very important as they can traumatize and devastate the limb tissues [17]. Soft tissues of the residual limb in the prosthetic socket perform several functions. First,

shear forces and pressure is applied with the help of the socket while it gets fitted on the residual limb. Second, rubbing of the skin against the interior surface and the edge of the socket edge may take place. Third, tissues of the residual limb will be repeatedly exposed to a high humidity environment because of the prosthetic socket being fitted well on the residual limb, thereby eradicating the capability of circulation of air and the concomitant entrapment of accumulated sweat. Fourth, the limb might undergo probable mechanical and chemical allergic reactions or irritations to a variety of socket materials [21]. Under these circumstances, tissue response to the shear and normal forces and to the outer forces, may exemplify many symptoms, such as deformation of tissue, interstitial flow of fluid, irritation, blistering, pain, ulceration, discoloration of the skin and many others [22, 23].

Based on all aforementioned understandings, the pressures could change with the residual limb shape/volume fluctuation while sweating/moisture could modify the friction coefficient. All these together could cause the shear stresses to fluctuate throughout the day depending on the patient's characteristics and responses and there is no information that informs us as to which combinations of these two stresses are acceptable for skin problem risk.

1.5 Current Shear and Pressure Sensors

As pointed out in the last section, due to the lack of understanding on the etiology of skin injuries, in this thesis, we focused on realizing a scientific instrument that can monitor both normal and shear stresses continually for enhanced prosthetic performance and long-term fitting. In accordance with that goal, there is strong need to develop a thin, light, compact and multi-dimensional sensor that is capable of measuring the shear and normal force with a high sensitivity, resolution, robustness, compact data acquisition

system wirelessly interrogated without needing a battery [24, 25]. In the last decade, various sensing techniques were developed. The majority of the sensors, however, can only measure normal forces and some of them can only measure plantar shear forces. Because of the aggregation of the proposed sensors individually for shear and pressure, we are mostly focused in this section on the sensors which are capable of measuring both shear and pressure simultaneously and asynchronously.

1.5.1 Strain-Gauge

The use of strain gauges for measuring shear and pressure stresses of lower limb prostheses was established late in the 1960s by Appoldt et al [26]. In 1980 TAPPIN et al presented a single-axis sensor (piston-type sensor) which would measure shear stresses. Soon, in 1992, two-axis shear measurement sensors came out enhancing the components and design, and then, the third-axis was included to measure both normal and shear forces accurately as developed by Williams et al. The disadvantage of piston-type strain gauge sensors was the error generated in measuring the shear sensing axes due to temperature sensitivity and the guage's bulky size [27]. Later, Sanders and Daly used a different mounting method allowing for the measuring of stresses simultaneously with strain gauge sensors in three orthogonal dimensions in which the instrumentation error on the average was less than 4.2% full-scale-output (FSO) for normal measurements in three orthogonal direction and less than 0.9% (FSO) for shear measurements in two orthogonal direction during walking [28, 29]. Afterwards, several scientists developed and improved strain gauge in-socket-wall sensor designs that contributed to a better understanding of stresses in the interface of prosthetic sockets [30, 31]. Strain gauge type sensors, developed by Sanders, needed to be drilled to mount into the socket wall, which could change the pressure distribution. On the other hand, for

this type of sensor, experimentation is conducted in the laboratory, as this sensor needs more power to function and therefore, could not be considered as a clinical device [32].

1.5.2 Piezoresistive

It has to be pointed that, there is no reported simultaneous shear and pressure sensor using piezoresistive technology. The Rincoe Socket Fitting and F-Socket systems which are based on printed circuit board technique, are the most generally used piezoresistive sensing sheets for interface pressure measurement inside prosthetic sockets [28]. In 2001, a microfabricated sensor for shear stress was developed for measuring the stress between stump skin and the hard socket of the prosthesis [33] with an hystersis error of 3.5%. The main purpose of this sensor was to examine the friction present at the surface of skin, which might harm the tissues and have an effect on their regular functioning.

1.5.3 Capacitive

In 2015, Laszczak and his colleagues developed a new capacitance-based device which could monitor the mechanical stresses present in the interface of the socket and the stump of an amputee's lower-limb, simultaneously. This sensor also demonstrated high linearity (approx. 5-8%), high pressure (approx. 1.3 kPa) and shear (approx. 0.6 kPa) stress resolution performance [34, 35]. Later, several tri-axial stress sensors were proposed, but their use in prosthetic sockets was limited due to their hard substrates that were not compatible with the residual limb, and also difficult and expensive to fabricate. The main disadvantage of this type of sensor is their propensity and susceptibility to crosstalk from noise and moisture. Therefore, they need sophisticated electronics to cope with this noise problem [28, 36].

1.5.4 Fiber Optic

A polymer based sensor, competent of measuring shear and normal stresses, was developed. This sensor contains two polymers implanted in a soft matrix. One is placed horizontally while the other is tilted transversely to the matrix. In spite of its high sensitivity, this sensor is appropriate for low normal stresses which is a limitation for practical applications [37]. Later, an opto-electronic sensor based on PCB was developed for measuring shear and pressure for prosthetic research. This sensor is made of an external silicone structure and a PCB board that provides accommodations for an array of sensitive elements which include a light transmitter, an LED, a receiver and a photodiode. This sensor works based on silicone deformation during the change in shear and pressure stresses. In 2012, Sandia's group developed a low-cost three-axis optoelectronic sensor based on multiple layers of silicone elastomer with small integrated circuits. This unique sensor was able to measure three different directions of normal pressure and horizontal and vertical shear forces and shear measurements [38]. This group uses an automatic adjusting system for the socket, that works by moving fluid into the bladders inside the prosthetic liner, which could be the source of damage to electrical components during testing. In addition, their full functioning might be hindered because of their frangibility and susceptibility to EMIs [28].

Due to the obvious limitation of all of presented sensors, which is wire connection and bulky interrogation system, these sensors are not suitable to be implemented in prosthetic device application.

1.6 Different Sensors Mounting and Fabrication Techniques

Successful integration of sensors into the prostheses would be an important focus for current prosthetics projects. To measure shear and pressure distributions,

sensors need the high capability and also spatial resolution to measure simultaneously both shear and pressure stresses. In most proposed sensing systems until now, shear and pressure sensors are mounted on the outside or inside of the socket or embedded into the socket wall. Based on the literature, few of the researchers tried to mount or embed the sensors on to or into the prosthetic liner respectively.

As mentioned before, most of the proposed sensors have bulky size which demands they be integrated outside of the socket. The technique of mounting sensors on the socket wall was first used in 1986 by Appoldt et al [26]. Subsequently, many researchers have used this mounting technique during the past five decades for their prosthetic socket fitting systems [30, 39]. In this method, for integrating the sensors on the socket wall, some modifications like drilling the holes or engraving the inside of the socket to locate the sensors are required which is difficult and may change the residual limb-socket interface distribution in different points and affect the accuracy of measurements [28].

Some researchers from Centre for Applied Biomechanics (CAB) at the University of Malaya, Malaysia, are developing a technique to embed the sensors into the socket wall. Using an injection method for fabrication of a custom-made socket is a complex technique [40]. Special high-temperature materials have to be used to avoid damaging of the sensors in the melted resins during cure time. On the other hand, the necessary sandwiched shape of the sensors between the hard material of the socket wall dismisses the accurate amount of interference stresses which leads to lower spatial resolution. Therefore, instruments that use these techniques have major shortcomings that limit their applicability to measuring shear stress distributions at the skin-prosthesis interface.

In the other technique, the sensors are integrated inside of the socket, there is no need to modify the shape of the regular sockets as the sensors have to be thin enough. If not, again that will affect the interference distributions [28].

In some of latest studies, sensors are embedded into an additional gel layer between the socket wall and the residual limb. However, gel liners alone do not guarantee comfort. Therefore, researchers use additional approaches, like modifying the sensor's locations and adding more gel layers between the residual limb and the hard socket to reduce unreasonable pressure of the sensors against the residual limb [41].

1.7 Proposed Shear and Pressure Sensors and Fabrication Technique

Our team proposed a shear/pressure sensor based on the electromagnetic interference principle of microstrip patch antennas [42, 43]. This sensor consists of a microstrip patch antenna and a U-shaped reflector separated by a dielectric superstrate. A microstrip patch antenna is an Electromagnetic (EM) resonator that can radiate or receive EM signals at two fundamental frequencies, and which consist of three components: a radiation patch, a dielectric substrate and a ground plane. When pressure or shear forces are applied to the sensor package, they lead to deformation of the superstrate and thus changes the vertical and/or lateral positions of the U-shaped director. Due to the EM coupling between the radiation element and the U-shaped director, the resonant frequencies of the patch antenna are influenced by the vertical distance between these two components as well as their lateral alignment. Therefore the shear and pressure displacement can be detected by monitoring the antenna resonant frequencies [43]. By implementing the proposed sensor for stump-socket stress monitoring, the microstrip patch antenna and U-shaped reflector will be separated by a layer of prosthetic liner material. The proposed antenna sensors - which are constructed

on flexible materials with a new design and existing in a layer of liner material - could be either inserted inside the socket and integrated with the commercial prosthetic liner or embedded in a custom-made prosthetic liner.

1.8 Advantageous of the Proposed Antenna Sensing Prosthetic Liner

It has to be pointed that the proposed shear/pressure antenna sensor by our group is light weight, compact in size, has multiplexing capability and can be wirelessly interrogated. In addition, the advantages of the proposed smart sensing prosthetic liner over conventional smart socket device are summarized as follows:

- Compatible to the skin: The liners with embedded antenna sensors are compliant with the shape of the residual limb.
- High accuracy, sensitivity and resolution: Embedded antenna sensors have a very high accuracy over a wide range when compared to conventional socket mounted sensors.
- Mechanical properties and flexibility: Our smart sensing liner is entirely made of soft and flexible materials when compared to current sensors which are typically made of brittle materials. In addition, our liner with embedded sensors maintains its workability while keeping the system flexible.
- Low fabrication cost: The material and facilities that are used for fabrication of the antenna sensors, and the expense of embedding them into the custom-made liner, are inexpensive.

1.9 Thesis Indexing

Chapter 1 provides an introduction to Prosthetics, its history, user problems and an overview of previous attempts to enhance the prosthetic socket performance and fit.

Chapter 2 discusses the basics of microstrip patch antenna theory and the analyzing of the antenna sensor using the transmission line model. The proposed shear/pressure antenna sensor by our group is explained and implemented. The antenna as shear sensor and reflector and as pressure sensor for in-socket application is also discussed.

Chapter 3 describes the design of a dual frequency antenna sensor, with and without the superstrate, using theoretical formulas and commercially available simulation software.

Chapter 4 describes the different fabrication processes for patch antennas. The procedures for selecting the appropriate silicone material for embedding the shear/pressure antenna sensor is also included. The measured radiation characteristics of patch antennas are also compared with simulation results from Chapter 2.

Chapter 5 describes the fabrication technique for embedding the antenna sensor in finished and real-size prosthetic liners.

Chapter 6 describes different options for implementing sensors in order to enhance the performance of antenna sensors.

Chapter 7 offers conclusions and Chapter 8 provides a brief description of projected future work.

Chapter 2

MICROSTRIP PATCH ANTENNA FUNDAMENTALS

This chapter provided some background information on the microstrip patch antenna and the fundamental parameters of the rectangular patch antenna. Moreover, analysis and the popular feeding techniques of the patch antenna are discussed. At the end, we discuss the ability of the patch antenna to measure the shear and normal deformations simultaneously with an aim to enhance prosthetic performance and fit.

2.1 History

The development of microstrip patch antennas are very interesting because they have a 60 year history. Many important advances in this technology have happened in the last two decades. The advent of the microstrip patch antenna concept has been credited to different sources and research publications [44]. The microstrip was originally proposed in 1952 by Greig and Englemann. Whether the invention of the transmission line had significant and long-lasting effects on the rapid development of microstrip patch antennas is debatable. The earliest “microstrip radiator” was conceived by Georges A. Deschamps and Sichak in 1953 at which time the microstrip antenna was integrated with the micrsotrip transmission line. Two years later, the first patented documentation of microstrip antenna design was proposed by Gutton and Baissinot in France [45]. However, neither Deschamps and Sichak’s paper nor Greig and Englemann’s proposed the microstrip patch antenna geometries as we know today, and in both cases, they introduced microstrip feed lines which developed new ways of thinking about complete antenna structures [46].

Some 20 years after the initial research, with the advent of printed circuit technology, the first practical microstrip antennas came into existence in the early 1970s, when conformal and low-profile antennas aerospace applications were necessitated by

the spacecraft and missile industry [47]. The microstrip patch antenna was initially fabricated by Munson in 1972 and subsequently reported in a journal paper by Howell in 1974. Howell presented the basic design procedures of rectangular and circular microstrip resonators (known as a microstrip antennas) and fed with a microstrip transmission line. Various microstrip geometries were developed by Weinschel in 1973 [48].

By the early 1980s basic microstrip antenna elements progressed in terms of design, analytical techniques and fabrication. In addition, the authors began improving microstrip antenna performance, and its applications were extended to many other technologies like radar, mobiles, robots and spacecraft, where size, weight and cost are constraints. Around this time, two books on microstrip antennas were published by Bahl, Bhartia & James and Hall & Wood, and extensive research publications regarding the development of microstrip antennas also followed by Dubost, which are still in current use today [49].

By the end of the eighties, there was a better understanding of microstrip patch antennas. In the nineties, microstrip patch antennas were being implemented in commercial application. By the start of the 21st century, microstrip antennas were very popular in mobile systems. At present, microstrip antennas remain the topic of many publications and are utilized in industrial development projects, contributing to continuous development in electronic system design.

The number of papers and articles published on antennas in the journals over the past ten years, attest to their importance. The microstrip antennas are the present day antenna designer's choice because of their numerous advantages, such as ease of integrations to system, analysis, fabrication, capability of dual and triple band operation, and its low cost and low profile [50].

2.2 Basics of the Microstrip Patch Antenna

The microstrip patch antenna in its simplest configuration is shown in Figure 2-1 (a), and consists of a very thin radiation patch on top of a dielectric substrate that has a ground plane on the underside. Both the radiation patch and the ground plane are made from a thin sheet of conducting material such as copper, silver or gold. The dielectric constant of the substrate plays an important role in the performance of the microstrip patch antenna, since; it affects both the width of the patch, which controls the input impedance and radiation characteristics, and the length of the patch, which controls the resonant frequencies of the antenna. Various mathematical models have been developed for the radiating element of the patch antenna, but the most widely used configurations are rectangular and circular. Figure 2-1 (b) shows some other configurations. Most of them are too complex to analyze or fabricate and need heavy numerical computations [45].

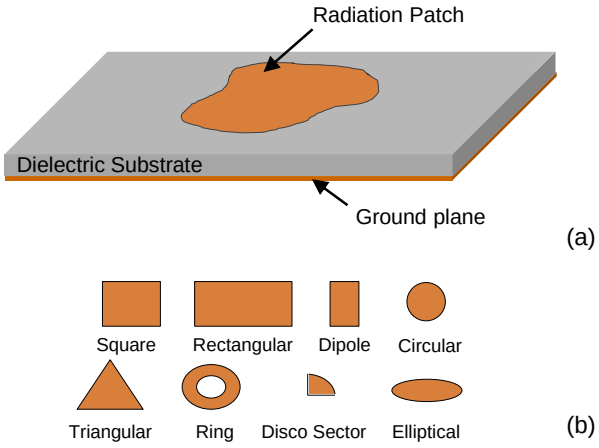

Figure 2-1 Microstrip patch antenna; (a) schematic diagram of microstrip patch antenna; (b) typical shapes of microstrip patch antenna

As shown in Figure 2-2, a rectangular microstrip patch antenna is defined by its length L and width W. The conducting patch does not form the radiating elements;

instead, the two edges of the patch L and W provide the radiation. For a rectangular microstrip patch antenna, the thickness of the patch t and the height of substrate h have to be much thinner than the free-space wavelength (λ_0) where the usual substrate thickness is about 0.02 λ_0 and in the range of 0.003 $\lambda_0 \leq h \leq$0.05 λ_0 (See Figure 2-2). In addition, the length of the antenna is mostly half a wavelength in the presence of the dielectric, and is normally between $\frac{\lambda_0}{3} < L < \frac{\lambda_0}{2}$. Various substrates can be used for microstrip patch antennas and the dielectric constant of them ε_r is generally in the range of $2.2 \leq \varepsilon_r \leq 12$ [51].

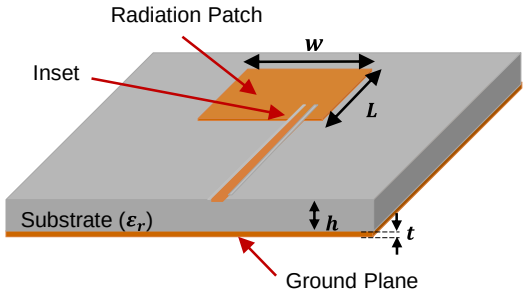

Figure 2-2 Schematic of rectangular microstrip patch antenna

2.3 Feeding Methods

There are many methods that can be used to feed microstrip patch antennas which can be categorized in two classes: contacting and non-contacting. The four methods of microstrip line, coaxial probe, aperture coupled feed (through the slot), and proximity coupled feed are considered as the common methods and are presented in detail in Figure 2-3. The role of feeding is very important to improve antenna input impedance matching and polarization characteristics [51], and therefore, critical for the efficient operation of an antenna. However, all of these methods have varying degrees of difficulty in their fabrication processes. Indeed, coaxial feed requires a hole, which has to be drilled into the substrate (see Figure 2-3 (b)). In addition, both methods of aperture

and proximity coupled feed methods require alignment for their multiple substrates which decrease the accuracy of fabrication (see Figure 2-3 (c) and (d)). In this thesis, a decision was made to use the microstrip line method by comparing different feeding methods. Therefore, in the next section, we focused on the concept of microstrip line.

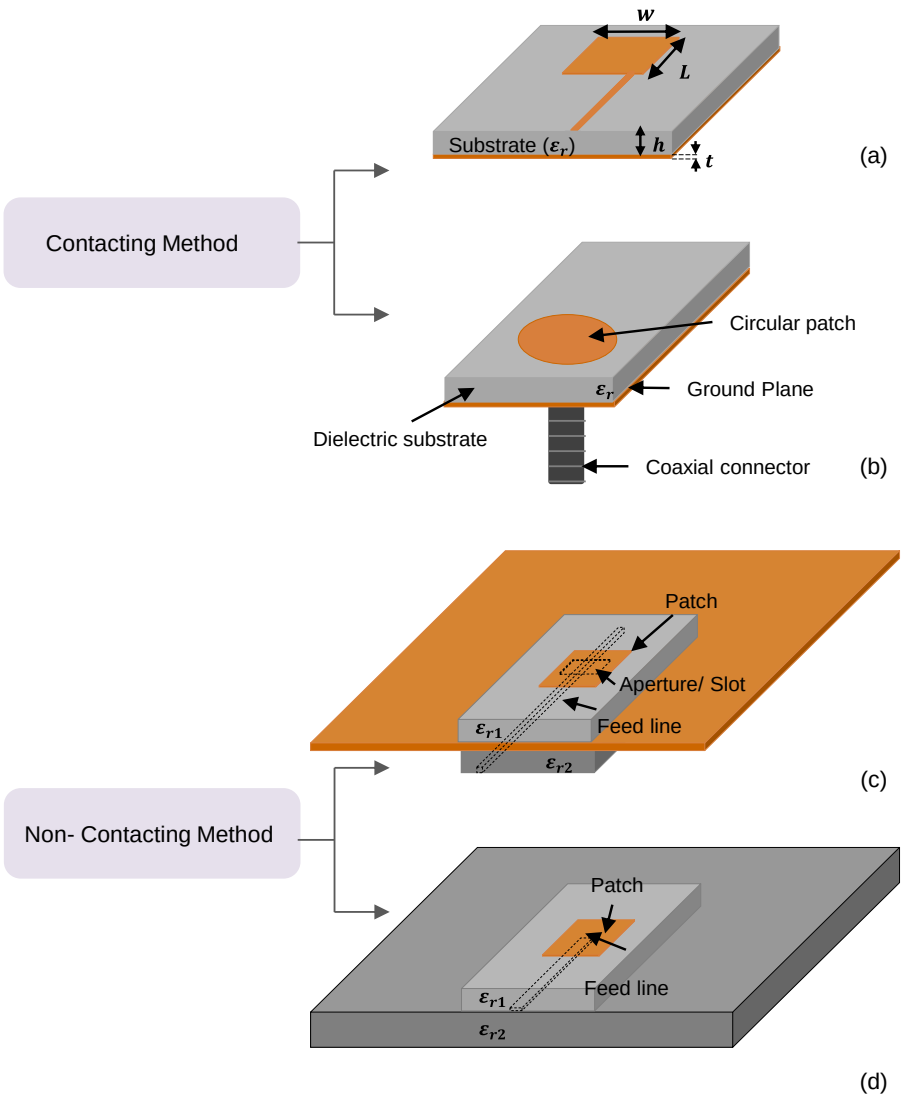

Figure 2-3 3-D view of microstrip antenna feeding methods; (a) microstrip line; (b) coaxial line; (c) aperture coupled feed; (d) proximity coupled feed [51]

2.3.1 Microstrip Line

Microstrip line is the simplest feeding method option. In this method, the feed line can be considered as a tailing of the patch and is connected directly to the edge of the patch. The width of the feed line is much smaller than the patch and very simple to match by adjusting the inset position [52]. In addition, the patch antenna can be matched to the feed line in two different ways; 1- Inset Feed (see Figure 2-2) and 2- Quarter-Wavelength Method which will be discussed in (Chapter 5, Part 5.1)

2.4 Microstrip Patch Antenna Analysis

There are many different and popular analytical models for a microstrip patch antenna such as transmission line model, cavity model and full-wave model. It is very simple to analyze the rectangular microstrip patch antenna using the transmission line model [51]. This thesis focus on fabricating thin and flexible shear and pressure antenna sensors, which could be compatible with the prosthetic liner, and the transmission line model is the most accurate one for thin substrates.

2.4.1 Transmission Line Model

The transmission line model is a low-impedance transmission line of a certain length l, two slots of width w and a height of h, which is connected to the patch antenna as shown in Figure 2-4. By studying the electric field propagation in the microstrip line, some of the electric field lines travel into the air instead of the dielectric substrate. Therefore, for accounting fringing and wave propagation, an effective dielectric constant ε_{reff} is presented which should be replaced with ε_r.

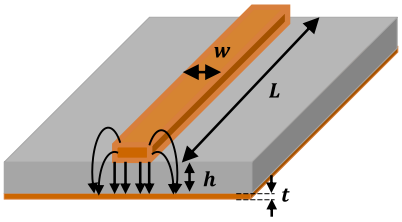

Figure 2-4 Electric field lines in transmission line

According to Figure 2-5, the fringing fields around the patch antenna help us to explain the radiation of the microstrip patch antenna. As the dimensions of the patch are finite along the length and the width, electromagnetic radiation happens primarily due to the fringing fields between the patch edge and the ground plane. Indeed, fringing is a function of the geometrical dimensions of the patch (L, W), height h and the dielectric constant of the substrate ε_r. The physical dimensions of a microstrip patch antenna would look smaller than the electrical dimensions because of the fringing effects [45, 51].

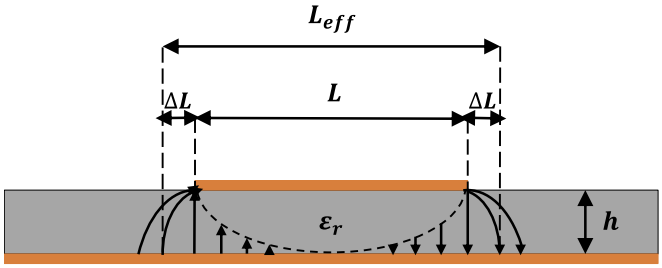

Figure 2-5 Fringing field for the dominant mode in a rectangular microstrip patch antenna

2.5 Shear and Pressure Antenna Sensor

Recently, our group demonstrated a shear sensor based on a microstrip patch antenna fabricated on a soft foam substrate with a slotted ground plane. The slot in the ground plane along the length of the patch antenna caused an obstruction in current movement along the width direction, forcing the current to flow around it. As a result, current along the width direction was enhanced which led to an increase in the electrical

length, thus reducing the corresponding resonant frequency f_{10}. Therefore, by applying shear, the foam material substrate will deform and cause a change in the overlapping length between the slot and the patch antenna that can be detected from the shifting of the antenna frequency [24]. After three years of using the same concept, our group presented a microstrip patch antenna sensor that is capable of measuring the shear and normal pressure simultaneously [43]. as stated in the introduction, we see that there is a strong need to improve socket design and shear-based dynamic fitting strategy. Over the past two years, our group began to present the implementation and characterization of a shear and pressure antenna sensor which is appropriate for measuring the in-socket interference at real-time. The patch antenna, and reflector characterization to detect shear and pressure simultaneously, are described in detail in this part and the design and fabrication of them are discussed in Chapter 3 and 4, respectively.

Based on the electromagnetic interference of multi-layer microstrip patch antennas, the shear and pressure sensor consists of a microstrip patch antenna, a soft dielectric material and a U-shaped reflector. The metallic reflector is separated from the patch antenna by elastic material which has a height h. Figure 2-6 shows a shear and pressure sensor based on a microstrip patch antenna in which the resonant frequencies of the microstrip patch antenna are dependent on the lateral and vertical position of the U-shaped reflector [53].

Our group, demonstrated that the shear and pressure displacements can be inversely measured from the measured frequencies of the patch antenna which will be discussed in detail in following section.

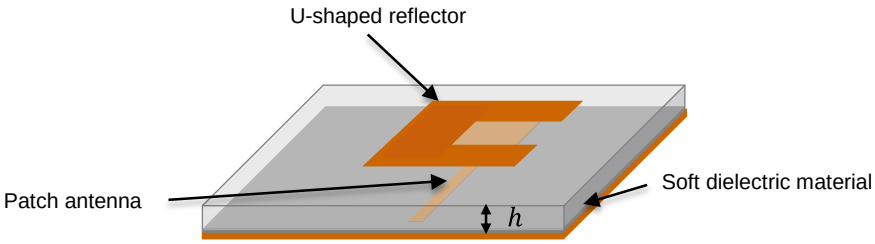

Figure 2-6 Multi-layer shear and pressure sensor

2.5.1 Patch Antenna as Shear and Pressure Sensor

As discussed before, both ground plane and the patch antenna comprise an electromagnetic resonator that can receive and radiate at certain frequencies that are defined by the patch geometry, the dielectric constant of the substrate, the substrate thickness and the properties of the electrodes. Any change in these parameters result in a change in resonant frequencies of the patch antenna.

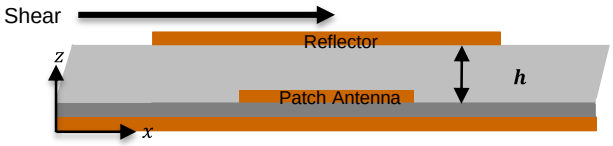

Figure 2-7 Lateral displacement between patch antenna and reflector due to shear deformation

As shown in Figure 2-7, shear force will change the lateral position of the reflector (in the x-direction) and the distance between the patch antenna and the reflector (in the z-direction). The distance between the radiation patch and the reflector h should be sufficient to prevent shear deformation in the y-direction [54].

The reflector can have different shape based on the application used, and the sensitivity of the shear and pressure antenna sensor could be adjusted by changing the shape of the reflector.

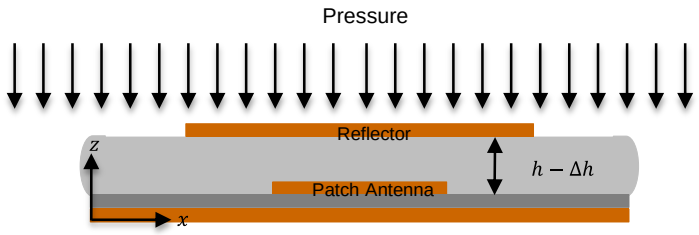

Figure 2-8 Vertical displacement between patch antenna and reflector due to compression

In this thesis, the reflector has a U-shaped metallic pattern situated on top of a thin and flexible sheet of dielectric substrate. The reflector is aligned at a point on the top of the patch antenna. After putting the reflector on top of the patch antenna, the electromagnetic wave radiated by the patch antenna will be reflected by the reflector and interfere again with the electromagnetic field of the patch antenna, This results in the shifting of the antenna resonant frequencies. As shown in Figure 2-8, normal pressure will reduce the height of elastic material following decreases in the distance between the metallic reflector and the radiation patch. Based on Figure 2-7 and Figure 2-8, the applied shear force and normal pressure can be detected by monitoring the measured antenna resonant frequencies [53, 54].

Chapter 3

SENSOR DESIGN AND SIMULATION

This chapter presents the design of a dual-frequency rectangular microstrp patch antenna with and without the superstrate. The procedures for initial design of microstrip patch antennas are provided, in this chapter. All parameters are calculated theoretically and described in details. For verification of the calculation, a MATLAB® code is used to determine the basic design factors of microstrip patch antennas. The MATLAB® code related to this chapter is available in [51].

For the simulation part, there are many different kinds of antenna design software which can be used for design and electromagnetic analysis of all types of antenna, but they all have various methods of analysis. For example, the High Frequency Structural Simulator (HFSS) is based on the finite element method (FEM), Microwave Studio (MAFIA-CST) is based upon Finite Integration in Technique (FIT) and EM (Sonnet pro) is based on Methods of Moment [55].

To summarize this chapter, the proposed antenna designs are simulated using HFSS and Sonnet software, both considered reliable. However, Sonnet can provide a user-friendly graphical interface, and for regular shapes like rectangular patch, the accuracy of Sonnet is higher than HFSS. Therefore, in this chapter, to avoid an increase in different simulation results, only the simulation results of Sonnet are presented.

3.1 Design of Rectangular Microstrip Patch Antenna

Based on the information in Chapter 2, the microstrip feed model as a feeding method and the transmission line model as a method of analysis, are selected for design of the microstrip patch antenna. The design of a microstrip patch antenna is an important key for the next steps in this thesis' objective.

For a rectangular patch antenna, the patch width has a small effect on the resonant frequencies. However, changing the patch width has remarkable effects on the power efficiency, input resistance and bandwidth. On the other hand, patch length determines the resonant frequencies and is very important in the design procedure. Resonant frequency of a rectangular patch antenna for TM_{010} mode is given by:

$$f = \frac{c}{2\,L_{eff}\,\sqrt{\varepsilon_r}} \tag{3.1}$$

where c is the velocity of light in free-space, ε_r is the dielectric constant of the substrate and L_{eff} is the electric length of the radiation patch. An effective dielectric constant is a function of frequency and as mentioned in part 2.4.1, it must be found because of the fringing of the cavity fields and wave propagation in the transmission line. The effective dielectric constant of the patch and the dielectric layer of air above it is in the range of $1 \leq \varepsilon_{reff} \leq \varepsilon_r$ which shows that the effective dielectric constant is slightly less than the substrate dielectric constant [56]. The ε_{reff} equation which is a function of dielectric constant ε_r, the thickness h of the substrate and the width of the patch W is expressed by Balanis as [51]:

$$\varepsilon_{reff} = \frac{\varepsilon + 1}{2} + \frac{\varepsilon - 1}{2}\sqrt{(1 + 12\frac{h}{W})} \tag{3.2}$$

The calculated effective dielectric constant is very critical for finding the electrical length and width. It has to be considered that for low frequencies the effective dielectric constant is essentially constant. However, for high frequencies due to more fringing effects, the electrical dimensions of the patch antenna look greater than its physical dimensions. For finding the effective length, the ΔL (Length extension) has to be determined which is a function of the effective dielectric constant and the width-to-height ratio ($\frac{W}{h}$), as shown in equation (3.3).

$$\Delta L = 0.412h \frac{(\varepsilon reff + 0.3)(\frac{W}{h} + 0.264)}{(\varepsilon reff - 0.258)(\frac{W}{h} + 0.8)} \quad (3.3)$$

Therefore, this value has to be added to the dimensions of the patch along its length on both side of the patch antenna. The effective length of the patch L_{eff} now becomes:

$$L_{eff} = L + 2\Delta L \quad (3.4)$$

where L is the actual length of the patch for a specified frequency. Finally, for an efficient radiator, a practical width at specific radiation frequency is given by Bahl and Bhartia as [45]:

$$W = \frac{c}{2\,fr}\sqrt{\frac{2}{(\varepsilon_r + 1)}} \quad (3.5)$$

The transmission line model is applicable to infinite ground planes only. But for fabricating the microstrip patch antennas, the ground plane has to be finite. Based on equation, it has been represented that if the size of the ground plane is greater than the patch dimensions, the results for finite and infinite ground plane will be the same [51]. Since, the ground plane dimensions would be given as:

$$L_g = 6h + L \quad (3.6)$$

$$W_g = 6h + W \quad (3.7)$$

In order to have an impedance matching for the patch antenna and excite the two radiation modes simultaneously, a feed inset y_0 is created. For an input impedance of 50 Ω the optimum feeding position (x_0, y_0) is calculated as:

$$x_0 = \frac{L}{\pi}\cos^{-1}\left(\sqrt{\frac{50}{R_{iny}}}\right) \tag{3.8}$$

$$y_0 = \frac{W}{\pi}\cos^{-1}\left(\sqrt{\frac{50}{R_{inx}}}\right) \tag{3.9}$$

The calculation of the resonant input resistances, R_{inx} and R_{iny}, are given by Balanis [51] as:

$$R_{in} = \frac{1}{2(G_1 \pm G_{12})} \tag{3.10}$$

where G_1 and G_{12} can be found in [51].

Table 3-1 Properties of $\mathrm{RO3003}$ Laminate

Properties	RO3003 (HH/HH)
Dielectric Constant	3.00 ± 0.04
Thickness (h)	$0.005''$ $(0.13\mathrm{mm})$
Copper Cladding	½ oz. $(17\mu\mathrm{m})$
Density	$2.1\ \mathrm{gm/\ cm3}$
Surface resistivity	$10^7\mathrm{M}\Omega$

The design procedures are outlined in Figure 3-1, with the assumption that the dielectric constant of substrate ε_r, the height of substrate h and the resonant frequencies are specified. A dual frequency patch antenna has been designed to operate at 6.1 GHz and 6.8 GHz with input impedance of 50 Ω, using Rogers ($RO3003$) substrate (See Table 3-1).

The $RO3003$® series of high frequencies circuit materials filled with ceramic PTFE-based laminate materials has the advantages of being having flexibility, low thickness, low cost, and light weight. It is easily cut and sewn, can be used in applications up to 30-40 GHz and maintain a stable range of dielectric constant versus mechanical properties and frequency, which is ideal for microstrip patch antennas.

The designed patch antenna is 14.25 mm in width and 12.6 mm in length. The feed width and inset are calculated to be 0.35 mm and 3.5 mm, respectively. The designed antenna is simulated using the EM simulation tool Sonnet Pro and Figure 3-2 (a) demonstrates the 3-D simulation model of the patch antenna with air layer on top and (b) corresponding resonant frequencies of the designed patch antenna. As the designed feed width is narrow for fabrication, the wider feed width of 0.4 mm is considered in the simulation.

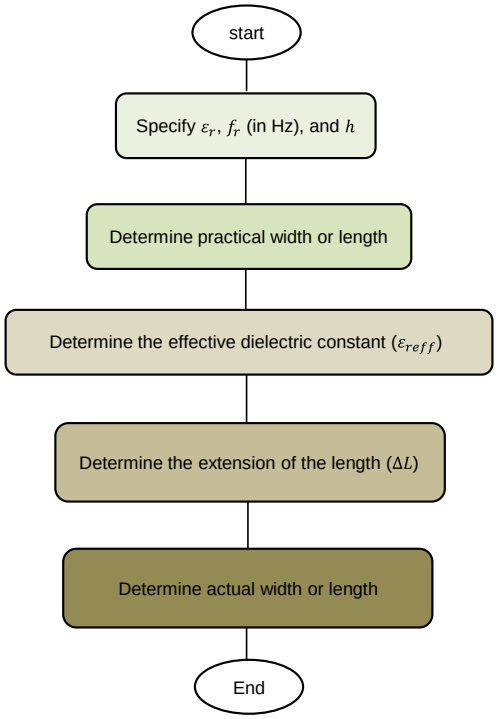

Figure 3-1 Typical design procedures for rectangular patch antenna

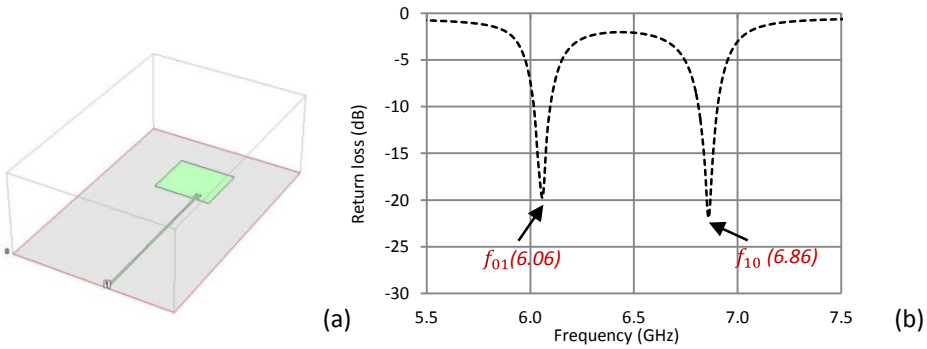

Figure 3-2 Microstrip patch antenna; (a) simulation model of a patch antenna; (b) simulated radiation characteristics of proposed patch antenna

Figure 2-1 shows the simulated S_{11} curve for a dual frequency patch antenna indicating f_{01} frequency is at 6.06 GHz with a return loss of -19.68 dB and f_{10} frequency is at 6.86 GHz with a return loss of -20.9 dB, which is compared with the desired frequencies of 6.1 GHz and 6.85 GHZ, respectively.

3.2 Design of Microstrip Patch Antenna with Superstrate

The multi-dielectric microstrip patch antenna shown in Figure 3-3 contains an addition of dielectric layers over the substrate. It is clear that covering the microstrip patch antenna with a superstrate will change the effective dielectric constant of the structure, which affects microstrip patch antenna properties like resonance frequency, gain and bandwidth, and these differences may completely degrade the antenna performance. On the other hand, with proper design at desired frequency of operation and choice of parameters, the performance of the antenna gain can be improved by covering the superstrate layer on the top of the antenna sensor. The only challenge of this section is to determine the effective dielectric constant of the multilayer structure which is required for design of the microstrip patch antenna for desired frequencies. The

antenna geometries' dependence of ε_{reff}, results in determining the dimensions of the patch antenna with high accuracy [57, 58].

It has to be mentioned that design and analysis of a rectangular microstrip patch antenna covered with superstrate can be carried out using different methods, such as, conformal mapping, the variational method, and the integral equation method (Green's Function). A common disadvantage of most of numerical methods is that they are an approximation and time-consuming [59].

.

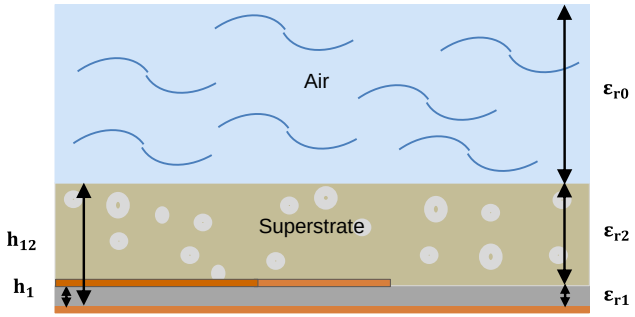

Figure 3-3 Side view configuration of a microstrip patch antenna covered with superstrate

In the following section, the method of conformal mapping used by Wheeler and Svacina is described for the microstrip patch antenna covered with a superstrate [59]. The relations of filling factors can be found with this method which will be discussed later. Then, the new calculated effective dielectric constant can be used to re-design and obtain the parameters of a new microstrip patch antenna.

It is obvious that a point in the w-plane can be linked to a specified point in the z-plane with a function which is called a coordinate transformation from the z-plane to w-plane. As shown in Figure 3-4, the layer of microstrip patch antenna, superstrate and air are transformed from the complex variable plane: $z = x + jy$ (see Figure 3-4 (a)) into

another plane: $w = u + jv$ (see Figure 3-4 (b)). We can see that with this method and a given function, a complex domain is transformed into a simpler domain and also the shape is conserved during transformation [60].

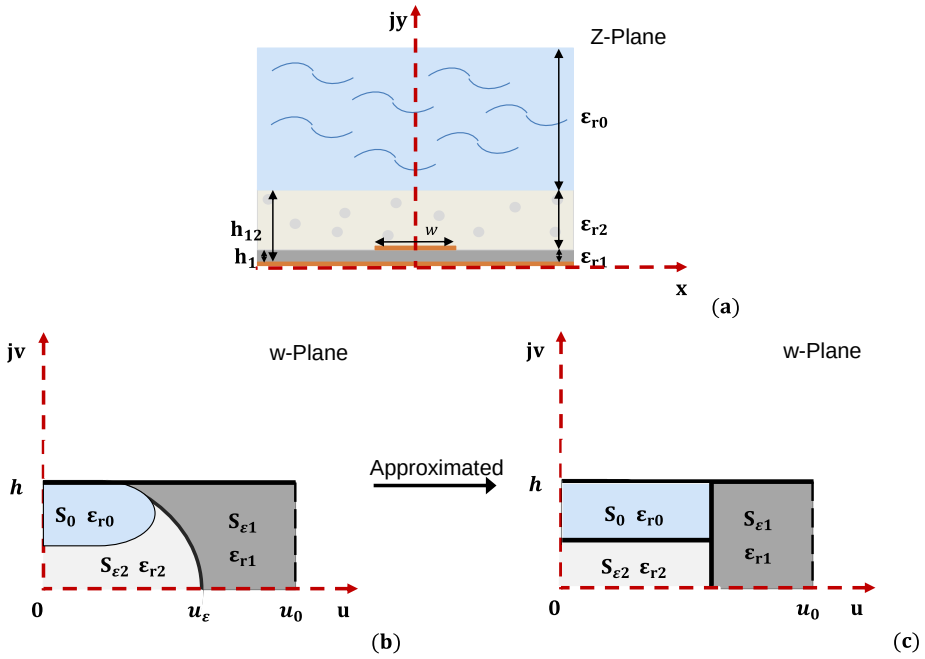

Figure 3-4 Conformal mapping process of a multidielectric rectangular microstrip patch antenna

In the cross section of w-plane Figure 3-4 , the ratio of each area of $S_{\varepsilon1}$ and $S_{\varepsilon2}$ for individual layers to the whole area S_t is defined as filling factors q_1 and q_2, respectively. Since, we have:

$$q_1 = \frac{S_{\varepsilon1}}{S_t} = 1 - \frac{S_0 + S_{\varepsilon2}}{S_t} \tag{3.11}$$

$$q_2 = \frac{S_{\varepsilon2}}{S_t} = 1 - \frac{S_{\varepsilon1} - S_0}{S_t} = 1 - q_1 - \frac{S_0}{S_t} \tag{3.12}$$

After approximating the boundary curves of areas S_0 and $S_{\varepsilon 2}$ based on Figure 3-4, for a wide microstrip line ($\frac{w}{h} \geq 2$), the filling factors can be:

$$q_1 = 1 - \frac{1}{2}\frac{\ln(\frac{\pi}{h}w_{\varepsilon f} - 1)}{\frac{w_{\varepsilon f}}{h}} \tag{3.13}$$

$$q_2 = 1 - q_1 - \frac{1}{2}\cdot\frac{h - v_\varepsilon}{w_{\varepsilon f}}\cdot \ln\left[\pi\frac{w_{\varepsilon f}}{h}\frac{\cos(\pi\frac{v_\varepsilon}{2h})}{\pi\left(\frac{h_2}{h} - \frac{1}{2}\right) + \frac{\pi}{h}\frac{v_\varepsilon}{2}} + \sin(\frac{\pi}{h}\frac{v_\varepsilon}{2})\right] \tag{3.14}$$

where $w_{\varepsilon f}$ is the effective width of a transmission line, h is the height of substrate, v_ε is the quantity and h_{12} is the height of substrate plus superstrate [59]. Therefore, $w_{\varepsilon f}$ and v_ε can be calculated as:

$$w_{\varepsilon f} = w + \frac{2h}{\pi}\ln\left[17.08(\frac{w}{2h} + 0.92)\right] \tag{3.15}$$

$$v_\varepsilon = \frac{2h}{\pi}\operatorname{arctg}\left[\frac{\pi}{\pi\frac{w_{\varepsilon f}}{2h} - 2}(\frac{h_2}{h} - 1)\right] \tag{3.16}$$

Finally, the relation for the quasi-static effective dielectric constant from the arrangement in Figure 3-4 (c) can be expressed as:

$$\varepsilon_{eff} = \varepsilon_{r1}q_1 + \varepsilon_{r2}\cdot\frac{(1 - q_1)^2}{\varepsilon_{r2}(1 - q_1 - q_2) + q_2} \tag{3.17}$$

And the characteristic impedance can be determined by equation (3.18) [59]:

$$Z_0 = \frac{120h.\pi}{w_{\varepsilon f}\cdot\sqrt{\varepsilon_r}} \tag{3.18}$$

A challenges to these conclusions is that for this thesis the superstrate for a microstrip patch antenna is a prosthetic liner material and its property data range for dielectric constant was not known. As will be discussed in (Chapter 4, part 4.2.3), RTV silicone is one of the most popular materials for today's fabrication of prosthetic liners. By adopting the range of dielectric constant for RTV silicone material from Polymeric

Dielectrics Materials Handbook [61] which is (2.7 - 3.9 (Average 3.3)), the calculation of new dimensions for a microstrip patch antenna with superstrate is achievable and then this parameter could be adjusted in the simulation model to achieve a reasonable match between the simulation and measurement results.

To adjust the constant dielectric in the simulation model, three multidielectric patch antennas with different dielectric constants of superstrate ($\varepsilon_{r2low} = 2.7$, $\varepsilon_{r2avg} = 3.3$ and $\varepsilon_{r2up} = 3.9$) were designed based on the conformal mapping method which led to different patch antenna dimensions. Then, the output data from the simulation for each patch antenna was exported to an Excel file. These three-designed patch antennas were then fabricated using the photo-etching method. The transmission lines of the three patch antennas were connected to the SMA connectors mounted on Rogers ($RO3003$) laminate, and the S_{11}curves of each patch antenna sensor were measured using Vector Network Analyzer (VNA) (Rohde & Schwarz, ZVA 24). The comparison of simulation and measurement data for each of the fabricated patch antennas, guide us to the correct value of constant dielectric. As shown in Figure 4-4, in (Chapter 4; Part 4.1.2), agreement between simulation and measurement was more obvious in the case of the dielectric constant 3.3. It has to be mentioned that, in this part, we only need an approximation of the dielectric constant for the designed parameters. After finding the desired material for our prosthetic liner or custom-made liner, the exact dielectric constant of the material could be found from the data sheet or, in the worst case, from technical customer support services. That information will be different from silicone to silicone and from company to company, and the design parameters have to be adjusted based on the material that will eventually be used as superstrate for shear/pressure antenna sensor.

Finally, the designed patch antenna with the superstrate with dielectric constant of $\varepsilon_{r2} = 3.3$ is 13.6 mm in width and 12.25 mm in length. The feed width and inset are

calculated to be 0.35 mm and 3.5 mm, respectively. As the designed feed width is narrow for fabrication, the wider feed width of 0.4 mm is considered in the simulation. Also as discussed in Chapter 2, the reflector has to cover three edges of the radiation patch [43]. Therefore, the reflector design parameters include the U-pattern geometric parameters such as U-shape length and width, U-shape arm width, U-shape slot width and the initial position of the reflector relative to the radiation patch along the x-direction which are 18 mm, 27.2 mm, 13.6 mm and 6 mm, respectively. In addition, the initial position of the reflector is considering at the center of the microstrip patch antenna which the length of the reflector is twice the width of patch antenna and it will very easy to align them together for fabrication part. The design of patch antenna with superstrate and reflector are shown in Figure 3-5.

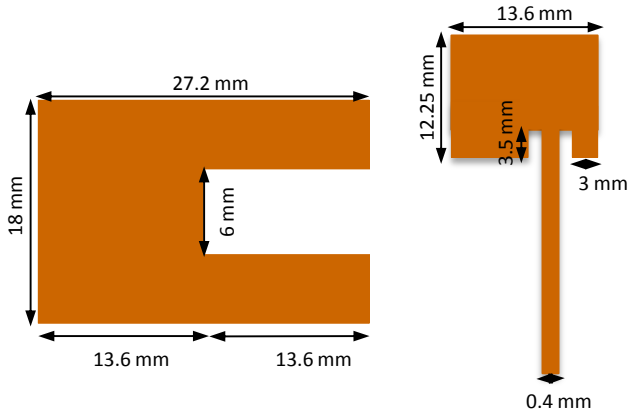

Figure 3-5 Design of patch antenna sensor and reflector (All dimensions are in mm)

Figure 3-6 (b) shows the simulated S_{11} curve for a dual frequency patch antenna with the superstrate layer ($\varepsilon_{r2} = 3.3$) and the reflector on top, indicating f_{01}frequency is at 5.97 GHz with a return loss of -13.9 dB and f_{10} frequency is at 6.85 GHz with a return loss of -29.1 dB, which is compared with the desired frequencies of 6.1 GHz and 6.85 GHZ, respectively.

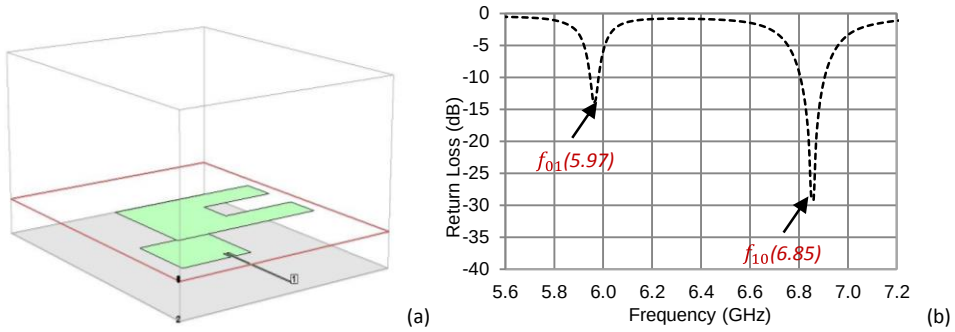

Figure 3-6 Microstrip patch antenna with superstrate; (a) simulation model of a patch antenna; (b) simulated radiation characteristics of proposed patch antenna

Chapter 4

SENSOR FABRICATION

Sensor fabrication on flexible substrates have earned growing attention with the rapid development of new applications where mechanical flexibility is important. Compared with conventional substrates, flexible substrates are more robust, of lighter weight and lower cost [62]. One of the easy ways to make the sensor flexible is to fabricate the sensor directly on thin and flexible substrates like Kapton® (Appendix A.1) or on very thin laminates like Rogers ($RO3003$) (Appendix A.2). Vacuum lamination is used on the former and the photo-etched technique is implemented on the latter.

In this chapter, we are looking into the details of different and novel sensor preparation and fabrication, their experimental setup and procedures, as well as the selection and characterization of custom-made liner materials replacing commercial prosthetic liners. The chapter concludes with the comparison of experimental and simulated results. The fabrication of the antenna sensors was done with the dimensions presented in chapter two's design and simulation section. In order to validate the antenna sensor's performance and capability, the experimental results were compared with simulations presented in chapter 2 as well. Although the fabrication of custom-made prosthetic liners is time consuming and costly, the need for making them was made plain after bonding the shear and pressure antenna sensors on commercial prosthetic liners and not realizing the desired flexibility for application.

4.1 Microstrip Patch Antenna Fabrication

4.1.1 Fabricate Antenna Sensor from Kapton/Copper Films using Vacuum Lamination

The laminating technique normally consists of one or more substrates which can be combined using adhesives with the presence of heat or pressure. Vacuum laminating is one of the basic techniques employed to create pressure on layers during their cure

cycle. It is obvious that a surface has equal atmospheric pressure of (14.7 Psi or 30 Inches of mercury) applied on all sides, but when vacuum is generated on one side, the pressure will be increased on the other side. Vacuum lamination technique was developed for fabricating a variety of complex shapes and large components; however, one of the simplest and most useful molds is the flat one. A table covered with a smooth plastic can be utilized for this purpose [63].

Based on a preliminary study using the vacuum lamination technique, the components and materials for setting up the vacuum-assisted lamination system are then specified and reproduced in Table 4-1. In addition, Figure 4-1 shows the typical experimental setup for vacuum lamination technique.

Table 4-1 Used vacuum bagging equipment [64]

component	Used component
Vacuum bag	Stretchlon® 200 Bagging Film
Breather film	Breather (FIBER GLAST Company)
Release film	Nylon Release (FIBER GLAST Company)
Vacuum pump	1/8 HP Vacuum & Pressure Pump Combo (FIBER GLAST Company)
Vacuum fittings	Thru-Bag Vacuum Connector Quick Disconnect & Nipples Air Hose Assemblies
Mastic sealant	Gray Sealant Tape
Epoxy	System 2000 Epoxy & 2060 Hardener

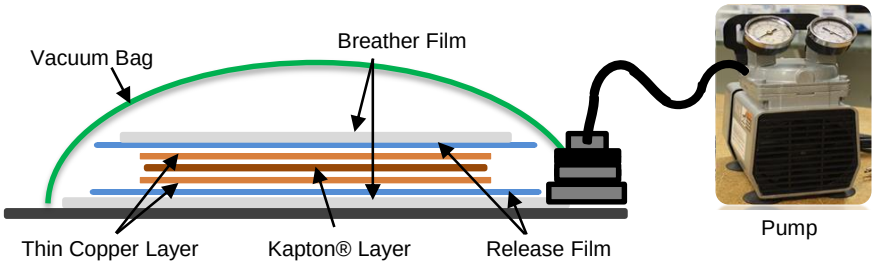

Figure 4-1 Basic of vacuum bagging assembly

The following section will discuss a step-by-step procedure to setup the vacuum lamination system for fabricating of the proposed microstrip patch antenna in chapter 2.

1. Materials for patch antenna substrate and conductive layer are selected: a flexible sheet of Kapton® HN (Thickness of 5 mil (0.125 mm) and dielectric constant of $\varepsilon_r = 3.4$) and a thin commercial copper foil sheet, respectively. Then, one layer of Kapton® and two layers of copper sheet are cut to measure $8\,\mathrm{cm} \times 8\mathrm{cm}$. Then, to improve adhesion, the surfaces of the copper and Kapton® layers are sanded and then are cleaned and dried (Kapton® film can be rinsed with acetone). Based on experiment, the best way is that firstly patterned patch antenna layout on of the copper sheets and then use both plastic and tape to completely cover the top and bottom copper sheet (see Figure 4-2 (b)).
2. The first layer of breather film is placed on the work table and then the first release film is placed on the breather film (Release film has to be smaller than the breath film) (see Figure 4-2 (a)). The vacuum bag is prepared and cut in a size that is bigger than the longest part we plan to fabricate.
3. The pot life of epoxy (system 2000) is one hour. This medium pot life hardener (2060) is ideal for fabrication since there is more working time which improves lay-up schedules and performance of the patch antenna. Then, according to the given ratios (by weight (100:27) and by volume (3:1)), the 2000 Epoxy and 2060 Hardener are mixed together. One side of the copper layers is wet out with laminating epoxy and the other side is covered with plastic based on procedure 1 to prevent covering the surface of copper sheets with epoxy. It is critical to check that there is no dry parts of epoxy and also important to remove all excess epoxy between the layers, because

if additional epoxy exists, the effect of the dielectric constant of epoxy will not be negligible. Then, the copper layers are aligned on the top and bottom of the dielectric substrate and the laminate is placed into the center of the setup [65].

4. The first layer on top of the patch antenna is a release film which air will pass through but epoxy will not stick to this film. Release film is soft and easily conforms to the patch antenna. The next is a breather layer which assures that the vacuum will be uniformly distributed over the whole surface of the patch antenna. Then the second layer of porous release film and breather are added on top of the setup.
5. The pump and vacuum fitting has to be assembled. Then, sealant tape is applied around the table work and the vacuum bag is placed on the sealant tape. The vacuum connector is also assembled in the corner (See Figure 4-2 (d)).
6. The vacuum hose is inserted into the pump and vacuum connector. The pump is turned on and the bag pulled down on the patch antenna layers. Everything is checked to confirm no leak in the system and when epoxy comes out it means that the system works perfectly (See Figure 4-2 (d)).
7. After 24 hours (curing time), the patch antenna laminate is removed from vacuum bag (see Figure 4-2 (e)).
8. Photo-etching is used to fabricate the microstrip patch antenna which will be discussed in detail in the next section (see Figure 4-2 (e)).

One of the main goals in using vacuum lamination technique was to minimize any voids (bubbles and wrinkles) in the buildup of layers. But in the fabricated sensor, some bubbles do exist between the layers. To be specific and based on gathered

information, bubbles are sometimes caused by air trapped in the nip or from shrinkage of the laminating adhesive as it cures, or perhaps from incomplete drying of the epoxy which can be solved by using a Spactula and uniform pressure on the layers.

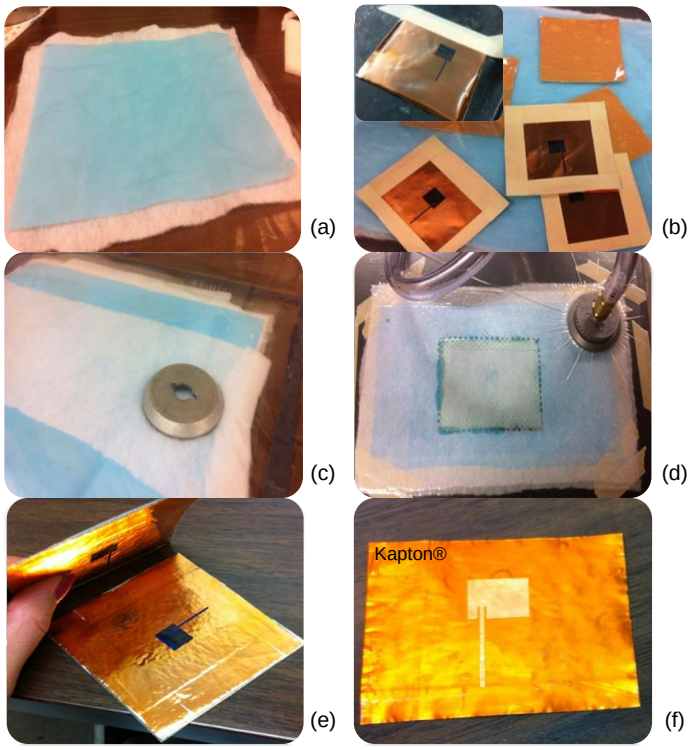

Figure 4-2 Fabrication steps of the patch antenna using vacuum lamination

After fabrication of the patch antenna, for the measuring of the radiation characteristics of the antenna sensor using a Vector Network Analyzer (VNA, Rohde & Schwarz, ZVA 24), the SMA connector was mounted to the end of the transmission line on the laminate board. To facilitate connecting an SMA connector on flexible substrates, it is better first to fix the SMA connector on the substrate by adhesive material (superglue) and then solder the center pin of the SMA connector to the transmission line.

As shown in Figure 4-3, the S_{11} parameters of the antenna sensor were measured using a VNA, although, the measured S_{11} parameter of the microstrip patch antenna indicates that the patch antenna has a satisfactory resonant response. But, repetition of the experiment to fabricate the patch antenna did not yield stable and repeatable results. There could be two reasons for this. First, as discussed in Chapter 2, by adding the adhesive layers in this technique, the resonant frequencies and gain of the patch antenna will be changed because of changing the effective dielectric constant. Secondly, even if we consider the adhesive layers as dielectric layers in the calculating design parameters, the thickness of the adhesive material is not controllable for different fabrication. Also, The fabricated sensor does not provide enough flexibility for application. Our next decision was to employ the commercial flexible laminate using photo-etched technique to reach the goal of project.

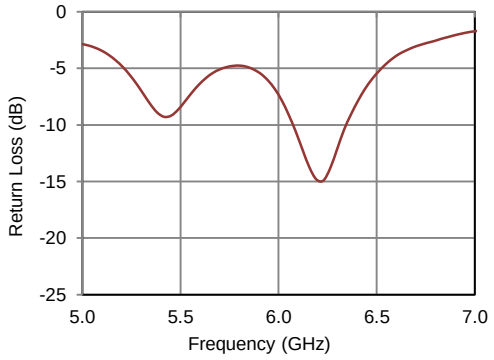

Figure 4-3 S_{11} parameter of the fabricated microstrip patch antenna using vacuum lamination technique

4.1.2 Fabricate Patch Antenna from Flexible Printed Circuit Boards

The photo-etched method is a chemical etching process which removes the unwanted material regions of the metallic layer, and is a very accurate method for

fabricating the proposed microstrip patch antennas and also the reflector mentioned in Chapter 2.

The antenna sensors and reflectors were fabricated on a Rogers laminate board ($\mathrm{RO3003}$) with a dielectric constant $\varepsilon_r = 3$ and 17.5 μm thick copper film on both sides. The designed layout of patch antenna and reflector were first printed on the Press-n Peed blue paper, and the laminate boards were cut into the desired rectangular pieces. Then, the Press-n-Peel Blue paper with the printed layout were ironed on to the laminate board. Since the used laminate boards are very thin, it is better to use napkin or a piece of plain paper between the iron and the laminate. The ground plane of the antenna sensor was left intact and covered with a tape. Then, the board was dipped in Ferric Chloride $\mathrm{FeCl_3}$ solution for twenty to thirty minutes to etch off the unwanted copper. The laminate is then rinsed in water to remove remaining etchant and then dried completely. The photo-etched fabricated rectangular microstrip patch antenna and reflector are shown in the Figure 4-4 (a). The S_{11} parameters of the patch antenna were measured and compared with the simulation results of the designed patch antenna in Chapter 2, as shown in Figure 4-4 (b). The resonant frequencies of the patch antenna are slightly lower than the simulated value which is 5.91 GHz for f_{01} and 6.7 GHz for f_{10}. The percentage error of both resonant frequencies is about 2.5 %. This discrepancy may be as a result of fabrication uncertainty (eg. the soldering of the SMA connector). Nonetheless, the measured data matched well with the simulation prediction.

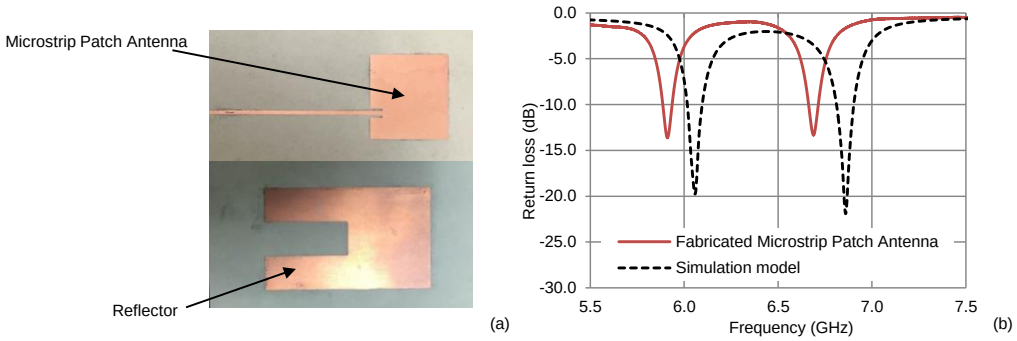

Figure 4-4 Microstrip patch antenna; (a) final photo-etched fabricated microstrip patch antenna and reflector; (b) comparison between measured and simulated radiation characteristics of fabricated microstrip patch antenna

4.2 Material Selection and Characterization

4.2.1 Commercial Prosthetic Liner Material

Three types of elastic materials, polyurethane (PUR), silicone, and thermoplastic elastomer (TPE) - with and without an outer layer of fabric - can be used to fabricate prosthetic liners. Each material has its own advantage and disadvantage as seen in Table 4-2.

Table 4-2 Advantage and disadvantage of the used elastic material for liners [66]

Material	advantage	disadvantage
Silicone	High stability Good adhesion Durable Easy to clean	Poor tear resistance Relatively high cost
PUR	Good pressure distribution Precise and comfortable fit Suitable for sensitive residual limb Inexpensive	Unreformable
TPE	Soft and highly elastic Contains skin-friendly oil Stretchable	Relatively expensive Viable just with fabric Sensitive to pressure Sensitive to temperature

Commercial prosthetic liners have differences in thickness, hardness, durability and cost and each company has its own formulation, description and characteristics. In this thesis, for fabricating the shear and pressure antenna sensor, the antenna is inserted inside the prosthetic liner and the reflector is placed on the outside of the said liner and is also aligned on top of the patch antenna. In this way, the U-shaped director is separated from the patch antenna using the prosthetic liner. We are grateful for the donated samples and assistance from colleagues from UT Southwestern who provided us with scraped prosthetic liners for study.

Table 4-3 lists information on the prosthetic liners gathered in the lab. As the Alpha Classic® prosthetic liner from WillowWood Company is most commonly used, it is selected for further study.

Table 4-3 Comparison of the available samples from different companies [67]

Company	Product	Liner material	Thickness (mm)	Peak Durometer OO	Falling Durometer OO
ALPS	Easy liner	TPE	6	29	0
OSSUR	Comfort	Silicone	6	39	3
OTTO BOCK	6Y70	PUR	6	48	7
WillowWood	Classic	TPE	6	29	0
	Hybrid	TPE	6	29	0

4.2.2 Integrating the Shear and Pressure Sensor in Commercial Prosthetic Liner

When comparing bonding methodologies for integrating shear/pressure antenna sensors, adhesive bonding offers great design flexibility and volume and weight economy, which are critical in our application. In this technique, intermediate layers of adhesive material are applied to connect substrates of different materials. For achieving a high bonding strength, the adhesive material type and thickness, surface preparation and curing process are very important.

- Surface preparation

Proper preparation of the bonding surface will greatly improve long-term durability of the adhesively bonded parts. Damaged points and unclean parts can create gaps and variable surfaces which can lead to non-efficient bonding. Once the surface is thoroughly clean, it can be covered with an adhesive of choice (Make sure the commercial prosthetic liner is clean, dry and free of substances and any processing lubricants).

- Adhesive material

The selection of the appropriate adhesive for this application is critical. The adhesive materials may consist of glues, epoxies or different substances which could cause two layers to adhere to each other by curing, pressure, or time. The crucial point is that the commercial prosthetic liner is commonly made by RTV silicone rubber which is extremely difficult to adhere to surfaces. We discovered that most adhesive materials like Super Glue, Gorilla Glue and 2000 Epoxy would not bond well with commercial prosthetic liners. All common adhesives remained on the substrate and it was extremely easy to peel off. Then we found out that, for adhering difficult substrates, primers are essential and are used to promote adhesion between nonbonding surfaces. $LOCTITE\ 7701$ active agent with $LOCTITE\ 7701$ instant adhesive (Medical Adhesive material) were the only products that could create a strong bond between the prosthetic liner and the patch antenna.

In order to fabricate a sample of a shear and pressure antenna sensor, the patch antenna and the reflector were fabricated on the thin and flexible Rogers ($R03003$) substrate. Then, the prosthetic liner, patch antenna and reflector were cut into the necessary rectangular pieces. These two parts and the commercial prosthetic liner were bonded securely together using medical adhesive material. First, the primer and the

adhesive material are applied to the patch antenna surface and inner side of the prosthetic liner (To ensure good bonding, the surface of the dielectric substrate were slightly sanded). Then, the microstrip patch antenna layer must be aligned to the commercial prosthetic liner before permanent bonding. Medical adhesive material will begin to cure in five minutes at room temperature under uniform pressure by hand. Great care needs to be taken when applying the bonding pressure in order to avoid substrate deformation. A similar procedure is used for bonding the reflector on to the fabric side of the prosthetic liner. The reflector was oriented in such a way that the center of the microstrip patch antenna was aligned with the center point of the reflector. A shear and pressure sensor was realized by fabricating the patch antenna and the reflector using a flexible electrical substrate material and bonding these two components on the prosthetic liner using medical adhesive material. The VNA (Model ZVA-24, Rohde & Schwarz) was programmed to measure S_{11} parameters from 5 GHz to 8 GHZ with a frequency resolution of 0.6 MHz (5001 points over 3 GHz).

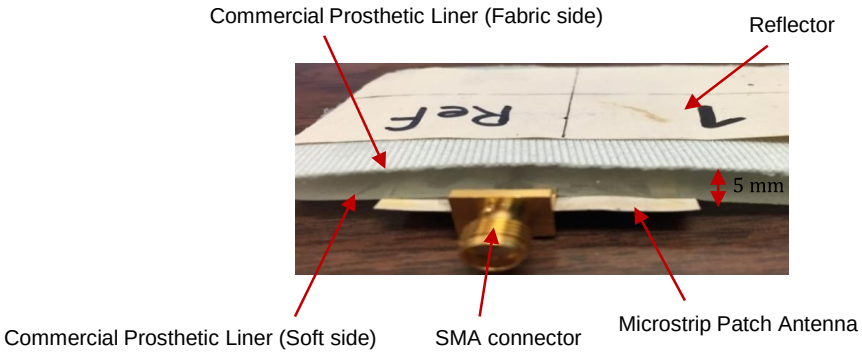

Figure 4-5 Shear and pressure antenna sensor bonded on commercial prosthetic liner

The S_{11} curves of fabricated patch antenna and shear/pressure antenna sensor and the simulation of shear/pressure antenna sensor are presented in Figure 4-6 in one graph. As expected from Chapter 2, the simulation predicts that the S_{11} parameters of a

shear and pressure antenna sensor will shift to the lower frequency after the liner material is placed on top of the patch antenna. As shown in the graph, the patch antenna displayed two resonant frequencies of 6.04 GHz and 6.84 GHz for f_{01} and f_{10}, respectively, and for the shear and pressure antenna sensor $f_{01} = 6$ GHz and $f_{10} = 6.77$ GHz. This prediction was validated by the measurement results for the sensor bonded on the commercial liner. The error sources, such as the fabrication, the soldering of the SMA connector, the solder ball capacitance and non-zero thickness of the adhesive material, could also contribute to these discrepancies. However, experimental results for the shear and pressure antenna sensor are presented in Figure 4-6 demonstrating the accuracy of the fabrication process and the validity of the proposed bonding techniques.

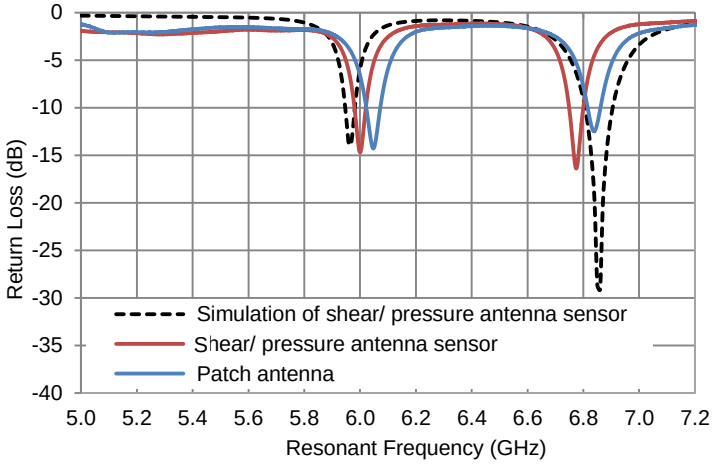

Figure 4-6 Comparison between the measured and simulated scattering parameters of shear/pressure antenna sensor bonded on commercial prosthetic liner

It has to be mentioned that the cured bonding layer of the medical adhesive material layer was a little stiffer than the liner, which could result in a decrease in flexibility of the sensor. In addition, we observed that the commercial prosthetic liner started to show signs of tearing, or debonding after several cycles of undergoing the

effects of shear and pressure. Therefore, we tried to find a silicone adhesive material especially made for silicone layers. There is a general rule which says that nothing sticks to the silicone except silicone. Sil-poxy from the SMOOTH-ON company is an adhesive material which can be used for bonding silicone for prosthetics and animatronics. As you can see in (Appendix A.5), the data sheet of the Sil-poxy states that it will work with tin or platinum-cure silicones and provides a strong, flexible bond between silicone parts with high elongation. According to the Sil-poxy product information, we expect that we could solve the problem of bonding the prosthetic liner to the patch antenna with a thin layer of the product. Unfortunately, the bond created with Sil-poxy failed and the product residue was easily removable from the prosthetic liner.

4.2.3 Custom-Made Liner Material

Although the fabrication of custom-made liners is time consuming and costly, their necessity was discovered after failed attempts at bonding the shear and pressure antenna sensors on commercial prosthetic liners. Based on information in Table 4-2, , the silicone material is selected as a soft material for custom-made liners. Actually, there are three common types of silicone rubber materials varying in their viscosity, curing temperature and methods (See Figure 4-7)

- ✓ High Temperature Silicone (HTV)
- ✓ Liquid Silicone Rubber (LSR)
- ✓ Room Temperature Vulcanization (RTV)

Solid silicone rubbers (HTV) are cured at very high temperature. Liquid silicone rubbers (LSR) are also cured at high temperature and widely used for injection method. Room temperature vulcanizations (RTV) are cured at room temperature and are available in a wide range of viscosities and hardness. RTV silicone material can be cured at room temperature and is therefore the best choice for facilitating the fabrication.

- RTV silicone material

RTV silicone materials based on catalyst are classified into two groups:

- ✓ Tin-based chemical (Condensation cure)
- ✓ Platinum-based chemical (Addition cure)

Each of them has its advantages and drawbacks. Tin silicone materials are easy to use and not costly, but they will become brittle over time and cannot be used for any purpose requiring flexibility and long shelf-life, which are important factors for this thesis. Moreover, tin-based chemicals are irritating to the skin. On the other hand, the platinum silicones are an ideal material for the casting method and remain flexible for years and are safe to use directly on the skin.

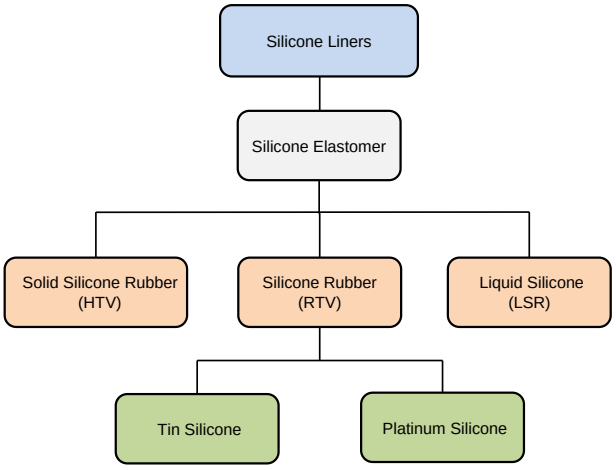

Figure 4-7 Flow chart of different classes of silicone material

Therefore, the platinum silicone is selected as a suitable RTV material for fabrication of custom-made prosthetic liners which exhibit a wide variety of shore hardness.

- Hardness of Silicone Material

One of the important parameters that has to be considered is the hardness of silicone material. In fact, hardness is the property of a material that enables it to resist plastic deformation, bending, scratching or cutting, which is an indicative measure of a material's texture and flexibility. The hardness of materials is most commonly measured by an apparatus known as a durometer, which provide an experimental hardness. Most of the prosthetic liner companies use extra soft materials for liner material, which is defined by shore OO. To find a close available commercial RTV silicone material to the base silicone material of commercial prosthetic liners, a digital durometer (Rex Durometer, Model 1600, and Type OO) was used for determining the experimental hardness of commercial prosthetic liners, resulting in a hardness of approximately 20 OO. Based on

Table 3-1, the average measured hardness of Alpha Classic® Wiloowood prosthetic liners is about 15 shore OO for which the peak durometer reading is 29 OO and the falling durometer reading is 0 OO. It has to be mentioned that during the process of measuring hardness, it is possible for the user to imbed the foot of the gauge into the test specimen and obtain false readings. Therefore, we have to consider an error range of 5 shore OO.

- Compression and shear properties of silicone materials

Our group implemented a test fixture for sensor characterization that could imitate the prosthetic socket and residual limb. As shown in Figure 4-8, a cantilever beam load cell was designed to be integrated with the test fixture. The cantilever beam has a slot at the center so that strain gauges bonded on the outer walls of the slot can have sufficient sensitivity to measure small compression and bending load changes. The test fixture was automated using two motorized translation stages and the plastic plate

attached to the bottom of the cantilever beam allowed for applying shear and pressure to the soft material while the top of the cantilever beam is fixed to the movable shear plate.

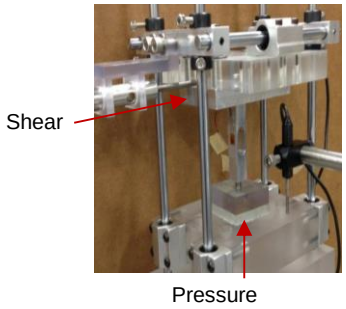

Figure 4-8 Test fixture for shear and pressure tests of soft silicone materials

All silicone materials of Table 4-4 were used to fabricate 41x41 mm^2 cubes with thickness of 5 mm. After curing, a digital durometer (Rex Durometer, Model 1600, and Type OO) was used for determining the experimental hardness of all samples and commercial prosthetic liners. Then, the cubes were tested in three different test conditions: (1) under pressure only; (2) under various shear displacements and a constant pressure of 13 psi; and (3) under various shear displacements and a constant pressure of 18 psi.

Table 4-4 Selected silicone materials for custom-made prosthetic liner (Appendix A.3)

Company Silicone Material	Material	Additive (Flesh 10)	Hardness	Elongation at break (%)
Bluestar	Sil4545	40 parts	35 (OO)	800
Bluestar	Sil4528	----	30 (OO)	800
Wacker	P 7671	----	21 (OO)	400
Wacker	P 7676	----	20 (OO)	700
Wacker	PK 16	----	15 (OO)	850

The displacement-pressure relationships of various materials are compared with Alpha Classic® WiloowWood prosthetic linear material in Figure 4-9 (a). The slope of the curve corresponds to the compression modulus of the material (i.e. Young's modulus). Similarly, the displacement-shear force relationships of various silicone materials are compared with Alpha Classic® WillowWood prosthetic liner in Figure 4-9 (b). The slope of the curve corresponds to the shear modulus of the material. Based on these two graphs, we found that the fabric laminated on the commercial liner alters the material properties of the prosthetic liner material significantly. Therefore, the selection of the silicone material was based on the material properties of the liner material with the fabric removed.

The materials with slopes similar to the Alpha Classic® WillowWood prosthetic liner were classified into the two groups: materials P7676 and PK16 from Wacker and materials Sil4528, Sil4540 and Sil4560 from Silbione. This material property data helped us to reduce the trial and error of embedding the antenna sensor in different silicone materials. PK16 had more similar slopes in both shear and compression testing to the Alpha Classic® WillowWood prosthetic liner, and was therefore selected as the silicone material to be used. In addition, it exhibited greater tear resistance and tensile strength due to additional cross-linking of its polymer chains.

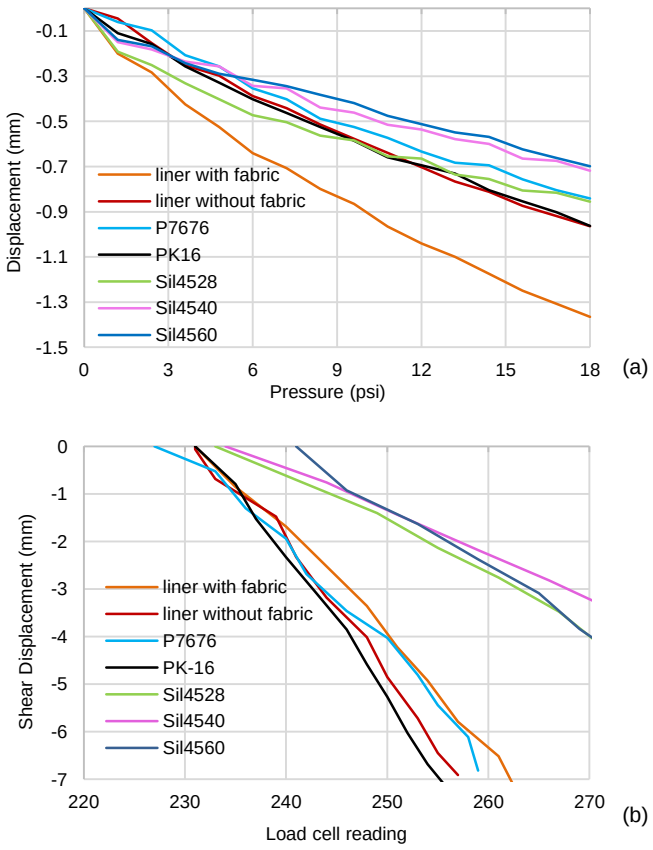

Figure 4-9 Characterizes the compression and shear moduli of silicone materials; (a) comparison of displacement-pressure relationships of different RTV silicone materials; (b) comparison of displacement-shear load relationship of different RTV materials

4.2.4 Custom-made Liner Fabrication Technique

In this part, different techniques are reviewed which could be used for making custom-made prosthetic liner based on the lab environment and the selected silicone material.

- Dip (Immersion) Technique

Dip coating is one of the oldest commercially applied coating processes which, at first glance, is rather simple. In the dipping technique, the uncured silicone is evaporated

and thereby concentrated which leads to it aggregating and finally drying to form the cured silicone. When the upward moving flux is balanced due to evaporation, the film position, and shape of the film profile, remain steady with respect to the coating bath surface. The solvent evaporates and drains and the silicone film acquires a wedge-like shape that terminates in a well-defined drying line. The thickness of the deposited layer is dependent upon the density and speed of the layers being applied [68]. Based on the literature review, in this technique, the plaster positive mold is covered by a special fabric (glass cloth). The fabric has to be covered by a primer to obtain high adhesion and then immersed into the molten silicone material. Also, the mold has to rotate until the hot silicone material has cured.

- Injection Molding Technique

Nowadays, injection molding is one of the popular methods in many markets. This method has the capability to fabricate complex shaped component with reasonably short cycle times. In this technique, the room temperature RTV silicone rubber has to be used. It is critical that the injection speed is high enough to ensure that the silicone material does not begin to cure before the hole is filled.

- Casting Technique

In casting techniques for small scale size, the cavity of the mold is filled with silicone material which then hardens. The only disadvantage of this method is cure inhibited by some surfaces, which can be solved by selecting the right plastics or 3-D printing material.

Based on the literature review, the dipping method is not an efficient method for fabricating uniform liners with a thickness approximating 5 mm, and it is also not recommended for use in a lab area since it needs a special boiler for heating the silicone material. On the other hand, injection molding also has size and shape limitations and

needs very expensive tools. Therefore, in this thesis, the casting method is selected as the appropriate method for fabrication of custom-made prosthetic liners. In the next part, this method is used for embedding one antenna sensors in the custom-made liner material.

4.3 Antenna Sensor Fabrication for characterization

A flat mold for embedding the patch antenna and the U shaped reflector in the custom prosthetic liner is designed using SOLIDWORKS and manufactured by UTA machine-shop (see Figure 4-10). With this mold, we are able to fabricate four antenna sensors simultaneously. The fabrication process is shown in Figure 4-10. First, a very thin layer of RTV silicone material is poured and completely cured in order to cover the ground plane side of the patch antennas. The prepared patch antennas are then placed on the edge of the mold. Next, a thickness of 5 mm of RTV silicone material is cast and the U-shaped reflector is aligned on the top surface of the cured silicone rubber. A thin layer with a thickness of 1 mm is subsequently cast to fix the alignment of the reflector on top of the patch antenna. This approach enables the placement of the reflector at selected distances from the patch antenna. After removing the liner material containing the embedded patch antennas from the mold, they can be easily cut into the desired shape, as you can see in Figure 4-10 (b).

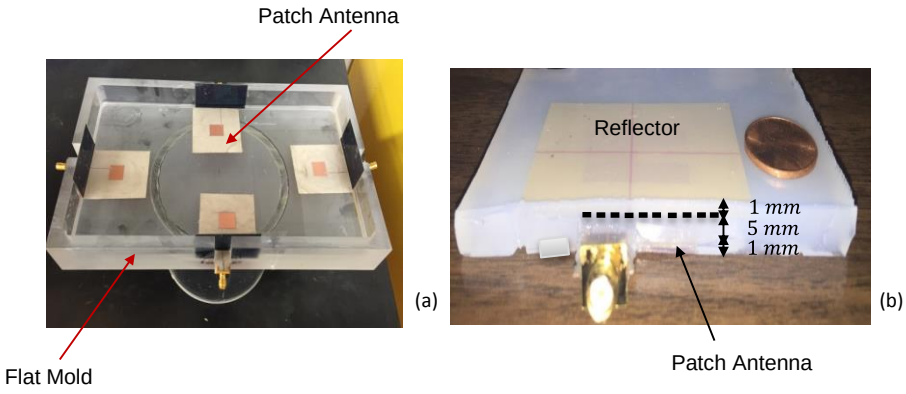

Figure 4-10 Shear and pressure antenna sensor implemented with soft liner materials as superstrate; (a) embedding Flexible patch antennas in 5 mm thick RTV silicone material using the flat mold; (b) flexible patch antenna embedded in 7 mm thick RTV silicone rubber

Chapter 5

IMPLEMENTING ANTENNA SENSORS IN CUSTOM-MADE LINER

This chapter describes the process of embedding two antenna sensors in a liner, one covering the area of the lateral tibial flare (LT) and the other covering the area of the medial tibial flare (MT). For this goal, we need the capability to embed the antenna sensor in arbitrary locations of the prosthetic liner, as determined by the load bearing location of the prosthetic. In the future, it will be required to use an array of antenna sensors to cover larger areas on the residual limb. In this chapter, the technical challenge of designing and fabrication of the microstrip patch antenna with long transmission line is described [69].

5.1 Long Transmission Line Antenna Design

As discussed in (Chapter 2; part 2.3), different feeding mechanisms can be used to excite a microstrip patch antenna. Feeding using microstrip transmission line results in a simpler antenna design and fabrication. However, the calculated width of a 50 Ω transmission line, for the thin and flexible substrate ($R03003$), is only 0.33 mm and such a narrow transmission line has poor performance and is difficult to fabricate using the photo-etched technique. To increase the width of the transmission line, we used the Quarter-Wavelength Matching Method (discussed below) to match the antenna impedance to a lower impedance, thus allowing for a wider transmission line.

5.1.1 Quarter-Wave Length Method

This method is named the quarter-wave length method, in which the input impedance is matched to the impedance ($Z_0 = 50\,\Omega$) of the transmission line. The quarter-wave transformer line is used between the 50 Ω transmission line and the patch for impedance matching. A transmission line with different length (one-quarter

wavelength) and different characteristic impedance, has to be designed to create the required impedance and match for the load (see Figure 5-1).

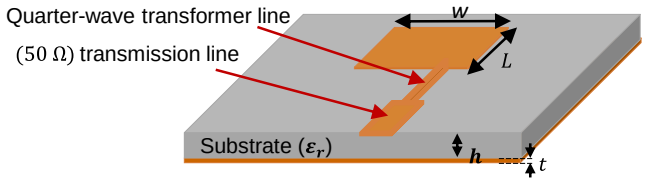

Figure 5-1 Microstrip patch antenna using quarter wavelength transformer

The impedance of the quarter-wave transformer is given by the equation (5.1):

$$Z_T = \sqrt{Z_0 * Z_p} \tag{5.1}$$

where the Z_T is the transformer characteristic impedance, $Z_0 = 50\,\Omega$ is the input impedance of the transmission line and Z_p is the impedance of the patch at the radiating edge, which can be calculated by the following formulation:

$$Z_p = 90\frac{{\varepsilon_r}^2}{\varepsilon_r - 1}\left(\frac{L}{W}\right)^2 \tag{5.2}$$

The width of $50\,\Omega$ transmission line can be calculated by using equation (5.3) given by Balanis [51], when $Z_T = Z_0$ or EM: talk calculator (Electromagnetics and Microwave Engineering).

After finding the transformer characteristic impedance from equation (5.1), the width of the quarter-wave transformer line can be found using the equation below:

$$Z_T = \frac{60}{\sqrt{\varepsilon_r}}\ln\left(\frac{8d}{W_T} + \frac{W_T}{4d}\right) \tag{5.3}$$

The length of the quarter-wave transformer line can be calculated by dividing the effective wavelength in the transmission line by four. It has to be noted that the wavelength in the transmission line is different form free-space wavelength (λ_0) and can be expressed as:

$$\lambda_{TL} = \frac{\lambda_0}{\sqrt{\varepsilon_{eff}}} \tag{5.4}$$

where λ_0 is the free-space wavelength and ε_{eff} is the effective dielectric constant of substrate [69].

If the antenna is successfully matched to the transmission line, we can then increase the length of the transmission line which is independent on the input impedance. If the match is not possible, the input impedance will change along the length of the transmission line and not enough power will be delivered to the antenna which will reduce the antenna performance. Therefore, achieving good impedance matching is particularly important, in order to obtain maximum radiated power.

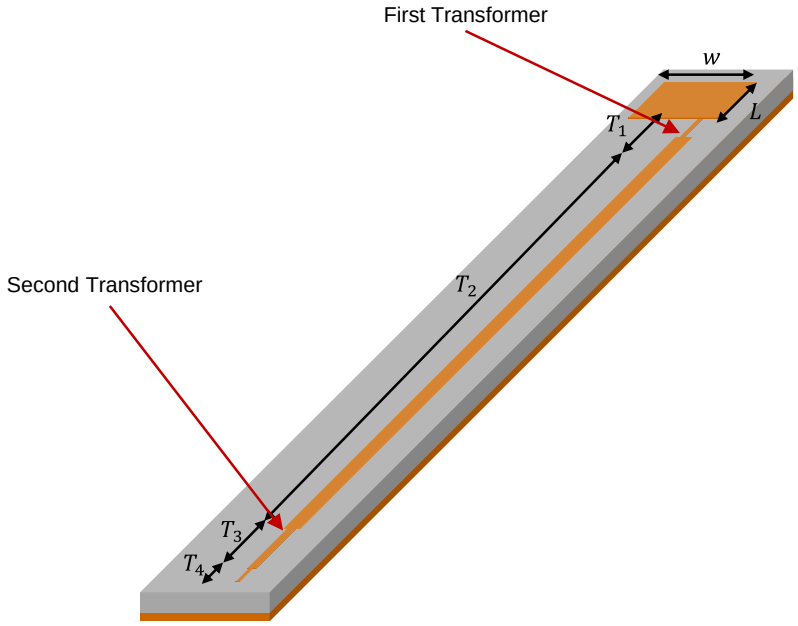

Figure 5-2 Model of long transmission line patch antenna; edge-fed with two quarter-wavelength transformer

According to the above equations, especially (5.3), if one transformer is used, the transmission line width will be smaller than 50 Ω transmission line (0.33 mm for flexible Rogers substrate ($RO3003$)). Therefore as shown in Figure 5-2, a microstrip patch antenna, using two quarter wavelength transmission line, must be designed in order to get the wider width for transmission line, thereby improving fabrication.

Input impedance of the patch at the edge was found to be $70\,\Omega$. This impedance is transformed to an impedance of $10\,\Omega$ using a quarter-wave transformer, which corresponds to a transmission line width of 1.8 mm. At the connector end, the impedance of the transmission line is again transformed by a quarter-wave transformer to match the 50 Ω impedance of the SMA connector. All of the calculated parameters of the designed long patch antenna are brought in Table 5-1.

Table 5-1 Designed parameter of long microstrip patch antenna

Parameter	With superstrate Size (mm)
L	13.6
W	12.25
l_{T1}	7.4
l_{T2}	200.5
l_{T3}	7.1
l_{T4}	3
w_{T1}	0.79
w_{T2}	1.8
w_{T3}	1
w_{T4}	0.33

Although, the calculated width of the feed line for a 50 Ω transmission line may sufficiently match the impedance, it is very difficult to fabricate and actually leads to an sufficient electrical connection between the transmission line and the SMA connector. Therefore, the wider width of 0.4 mm is chosen for fabrication. In order to verify the concept of the Quarter-Wavelength Method, the simulation model of the long antenna

design, built using an Electromagnetic (EM) simulation tool, Sonnet Pro, as well as the simulation radiation characteristics, are shown in Figure 5-3.

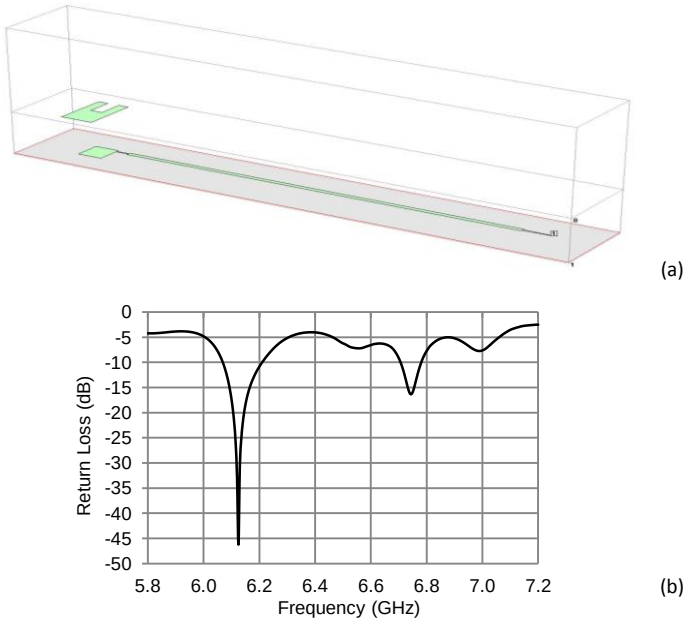

Figure 5-3 Antenna sensors with a long transmission line; (a) numerical simulation model of shear/pressure antenna sensor with two quarter-wavelength transformers; (b) simulated radiation characteristics of proposed long patch antenna

5.2 Long Antenna Transmission Line Fabrication and Measurement

A similar procedure as in (Chapter 4; part 4.1.2) follows for the fabrication of a long transmission line patch antenna as described in Figure 5-4 (a). When the fabrication is completed, the SMA connector is mounted on the feed line of the patch antenna. The electrical connection between the SMA and feed line is checked by a digital multimeter at the end of the SMA connector, before which the patch antenna is connected to the VNA (Model ZVA-24, Rohde& Schwarz) through a SMA connector.

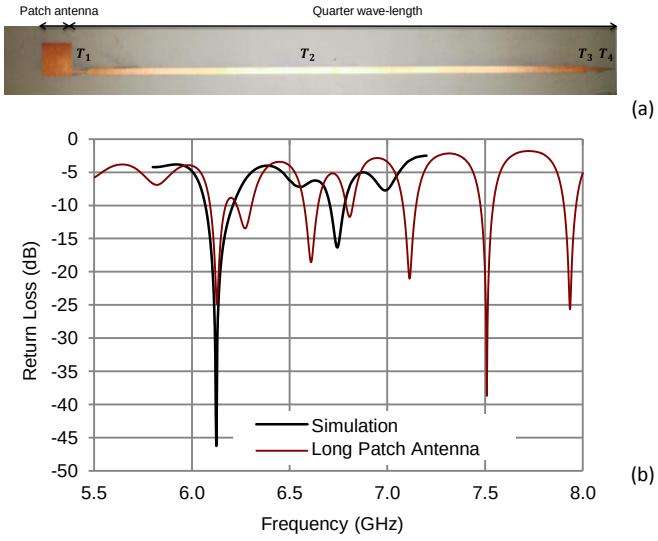

Figure 5-4 Long rectangular patch antenna; (a) patch antenna and transmission line fabricated on soft substrate; (b) comparison between measured and simulated S_{11} parameters

The S_{11} parameters of the patch antenna were then measured. As shown in Figure 5-4 (b), the S_{11} parameter of the fabricated microstrip patch antenna did not display two clear resonances, as predicted by the numerical simulation. By converting the S_{11} signal into a time-domain signal, we discovered that the additional valleys are due to the interference between the signals reflected at the connector and those reflected by the antenna patch (see Figure 5-5 (a)).

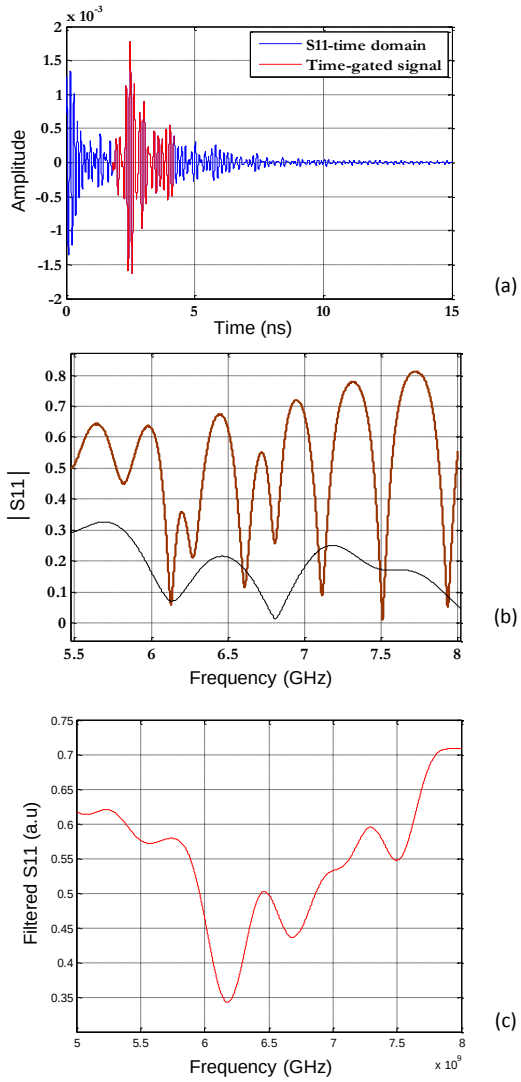

Figure 5-5 Characterization of the antenna sensor with a long transmission line; (a) S_{11} signal represented in time-domain; (b) Spectrum of time-gated signal; (c) Filtered S_{11} signal

The antenna mode radiation can be clearly observed starting at around 2 ns and finishing around 4.5 ns. If we use time-gating for the antenna mode signal to remove the signal reflected by the connector, and

process it with Inverse Fast Fourier Transform (IFFT), we can determine the antenna resonant frequencies from the spectrum of the time-gated signal (see Figure 5-5 (b)). The resonant frequencies agree with the resonant frequencies obtained from the Electromagnetic (EM) sonnet simulation model for long patch antennas. In addition, due to the long transmission line, the interference fringes are periodical with a high frequency component. Therefore, filtering the S_{11} signals using a low-pass filter can remove these high frequency components, as shown in Figure 5-5 (c). In the future, our group will use the portable FMCW interrogator to isolate the legitimate antenna sensor signals.

5.2.1 SMA Connector Stabilization

As our goal in this project is to test the smart prosthetic liner in a clinical setting, the flexibility and compability of the entire fabricated custom-made prosthetic liner, with the sensors on patient skin during testing, is very important. On the other hand, the reliability of the electrical connection, using a SMA connector, is very critical in determining the radiation characteristics of the antenna sensors. The radiation characteristics of patch antennas are measured using a VNA (Vector Network Analyzer). As well, during the walking of the patient in the clinical testing, loading, bending and movement are unavoidable That motion which could cause the SMA connector to move away from the feed line of the patch antenna or, in the worst case, to break the electrical connection between the SMA connector and the patch antenna. Both these problematics were ameliorated by designing two different supporters made of 3-D printed material (see Appendix B.2), in order to both protect the sensor against damage and also for stabilization and increased reliability of the results during the measurements of shear and pressure stresses in the clinical visit. In the first configuration, the supporter was designed for an SMA straight edge mount type with four legs which consisted of two parts with screw holes, and with the antenna sensor sandwiched between these two parts. The

two bottom legs of the SMA connector fit in the holes in the bottom part and the other two legs will go through the mold surface vertically. In addition, the bottom part is formed longer with a thickness of 0.05 mm - a little more than the edge of the liner - to protect the antenna sensor from damage from any impact on the end edges of the prosthetic liner. After soldering the center pin of the SMA connector to the end of the transmission line, the top part has to be aligned and screwed to the bottom layer. The aligned perpendicular plastic pin at the center of top part, is touching the SMA pin and the antenna sensor feed-line which could be help us to remain a good connecton by putting immense pressure on the solder contact during the test.Figure 5-6 (a) shows the antenna sensor and the SMA connector assembly in the first configuration.

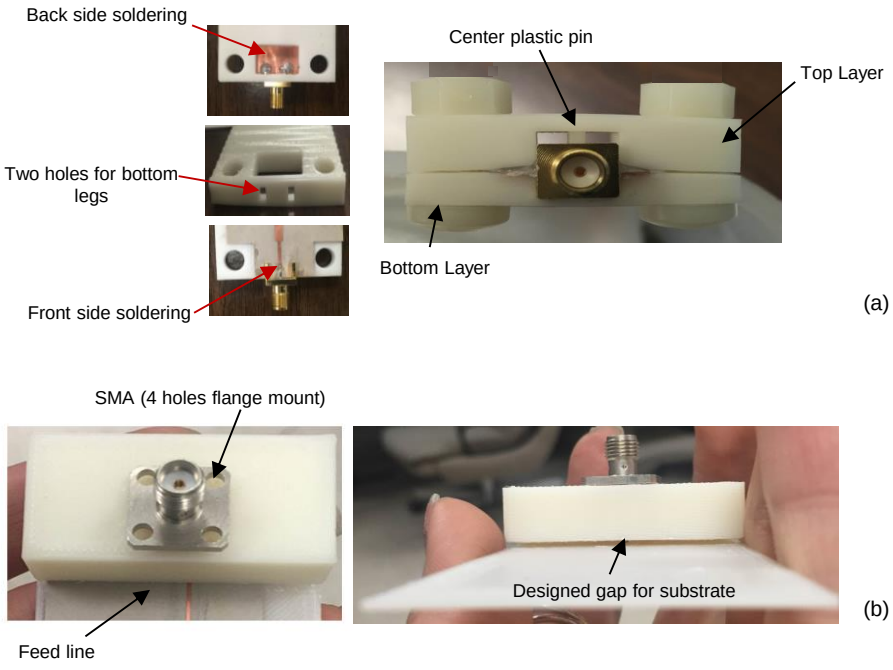

Figure 5-6 Antenna sensor and SMA connector fixture; (a) first configuration; (b) second configuration

In the second configuration, the support is designed in one part for an SMA connector with 4 holes flange mount as shown in Figure 5-6 (b). In this design, the gap allowes the laminate to pass through the mold. On the top side, four through holes are designed according to the SMA connector shape, in which the SMA connector can be set vertically with its pin the end of the microstrip feed line. In this case, the tip of the SMA connector can make contact with the feed line and be fixed by installing the screws and nuts. Theseimprovement could stabilize the measurement even with if the soldered connection came loose at the feed line.

5.3 Final Implementation of long transmission line antenna sensors in custom-made liner

In this part, the fabrication techniques are presented for embedding two antenna sensors in a custom-made prosthetic liner. The antenna sensors are embedded in a real-size custom-made prosthetic liner using two different techniques, which are discussed below.

5.3.1 First Technique: Casting the Liner using a Real-Size Mold

For real size prosthetic liner, based on the Alpha Classic Liners Sizing Guide (WillowWood,L), a nine-part mold was designed and fabricated using the 3D printing technique (see Appendix B.1). The design of the mold and a fabricated mold using 3D printing technology is shown in Figure 5-7 (a) and (b), respectively. The mold consists of an inner part which models a residual limb and an outer shell to model the prosthetic socket. The inner part is a tapered cylinder while the outer shell has four separable parts. When assembled, the inner part is centered inside the outer shell with a 6 mm gap between these two parts. As the 3D printed parts have tiny open pores, high grade sandpaper was used to polish the surfaces and high temperature spray (Heat resistant paint) was used to seal the pores. Prior to applying silicone, the surfaces were also

coated with a release agent - Ease Release® 200 - for easier releasing of the liner from the fixture.

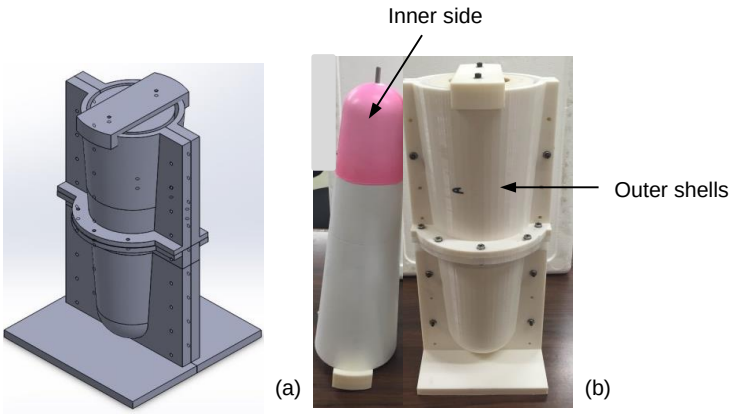

Figure 5-7 Embed antenna sensors in custom-made prosthetic liner (first technique); (a) design of the mold for liner; (b) Assembly of 3D printed inner and outer molds;

In this method, the alignment of the reflector and patch antenna is critical. If we fix the patch antenna on the inner side and the reflector on the outer side before fabrication, the alignment could fail with any small movement or if the inner side turns within the mold. Also, after pouring the silicone inside the patch antenna, the reflector can flow which again changes their alignment. Accordingly, the patch antenna was first coated with a layer of silicone material, both on the front and the back surfaces. The thickness of the coating on the front surface was 4 mm and the thickness for the back coating was 0.5 mm. In addition, the reflector is embedded in silicone material with a thickness of 1 mm on the front and 0.5 mm on the back. The patch antenna and the reflector were then aligned properly and fixed on the inner mold using a very thin layer of silicone material. This approach enables the placement of the reflector at selected distances from the patch antenna. Finally, the inner mold was placed into the outer mold and silicone mixture was poured to fill the gap between the inner mold and the outer

mold. Silicone is poured into the cavity between the cone and outer mold and allowed to cure fully. This method enables us to embed the antenna sensor in arbitrary locations of the prosthetic liner, as determined by the load bearing location of the prosthetic socket. To remove the cured liner from the mold, the outer shell of the mold is separated so that the liner can be released from the inner part. A picture of liner fabricated using this technique is shown in Figure 5-8. Two antenna sensors are embedded into the prosthetic liner. To put the liner on the limb of an able-bodied volunteer, the bottom of the liner was cut off. However, it was difficult to put the liner on using the conventional rolling technique because of the reinforcement for the sensor connector. In addition, the sensor could easily be broken if an attempt was made to fold the liner. So another method is used for fabrication of the liner in order to be able to characterize the fabricated antenna sensors on an able-bodied volunteer without damaging the antenna sensors.

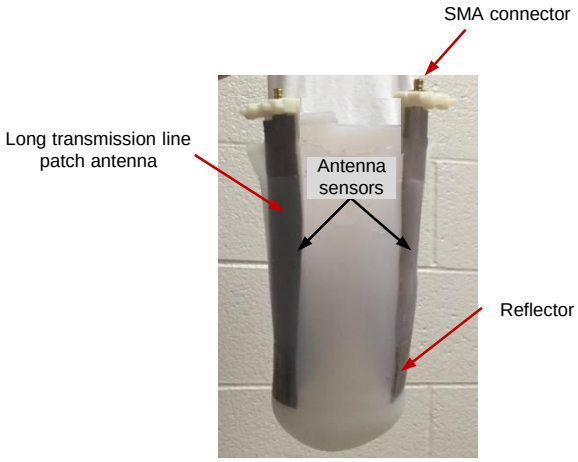

Figure 5-8 Fabricated prosthetic liner with embedded antenna sensors (first technique)

5.3.2 Second Technique: Casting the Liner in Sheet Form

In this method, a trapezoid mold was made to fabricate a sheet of silicone with the antenna sensors embedded, as shown in Figure 5-9. Prior to the casting, the locations of the antenna sensors, relative to the limber, were measured so that the

antenna sensors can be placed in the mold properly. After the silicone sheet was released from the mold, it was draped over the limb of the volunteer with the antenna sensors aligned at the desired locations. The silicone sheet was then trimmed and connected together using Velcro strips to form the liner, as shown in Figure 5-9.

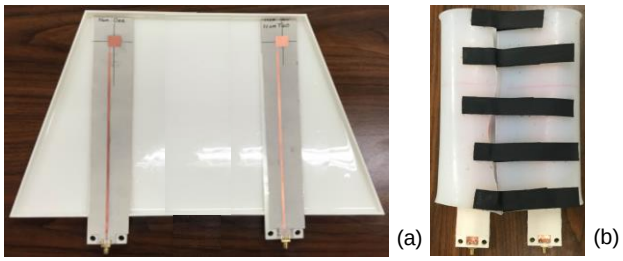

Figure 5-9 Embed antenna sensors in custom-made prosthetic liner (Second technique); (a) fabrication the liner in sheet form; (b) trimming and forming of the liner using Velcro straps

Chapter 6

ANTENNA SENSOR ENHANCEMENT

In this chapter, a novel approach is proposed to: (1) rectify the problem of breaking copper layer in the liner material through bending and (2) improve the flexibility of the patch antenna sensors. The first configuration studied was a patch antenna based on conductive foam/fabric. The second configuration was a complete fabric-based patch antenna. The fabricated antenna sensors - based on conductive foam and fabric - are a product with the conductivity of a radiator patch and the durability and flexibility of commonly used fabrics. In addition, a new design has been explored to increase the performance of antenna sensors using meandering line. The related design and fabrication processes in this chapter are very similar to previous cases, but some remarks are needed which will be forthcoming in details.

6.1 Electrode Material

There has been growing demand today for flexible portable wireless communication devices and the study of wearable flexible antenna sensors has been widely presented in recent papers [62]. Although in this thesis, the fabricated patch antenna on RO3003 are flexible enough and bendable, yet a thin copper layer of patch antenna can become brittle and easily broken after bending in a prosthetic liner when the liner is worn using the conventional rolling technique. This gave us a foundation to do work on patch antennas, taking conductive foam and fabric as electrode material, in order to facilitate the antenna's integration into prosthetic liners. We were also able to compare their performance with traditional copper patch antennas. These materials are much more durable, flexible, stretchable, and breathable than copper films and thus are more suitable for prosthetic applications. The fabrication of conductive foam and fabric

sensors, employed as a surface electrode of a patch antenna, are shown and discussed in the following section. They are non-allergenic and can be placed in contact with human skin.

6.1.1 Flexible Conductive Foam/ Fabric Antenna Sensors

We discovered that conductive foam and fabric could serve as electrode material for the antenna sensor. In order to evaluate their flexibility and capability as well as characterizing the antenna sensor's performance, three different prototypes of the antenna sensor with conductive foam (based on Kapton and PTFE substrate) and conductive fabric (Based on PTFE substrate) were fabricated. The fabricated antenna sensors' radiation characteristics were then analyzed and compared.

The commercial EMI Shielding conductive foam was chosen from Waveseal Company (Appendix A.4) due to its efficient shielding effectiveness, good balance of physical, chemical and electrical properties over a wide frequency range of 10MHz-10GHz, and its thickness (< 1mm). Moreover, having low dielectric losses and not absorbing moisture, both characteristics improve the efficiency and make them suitable for wearable applications. Tin/copper coated conductive fabric (LessEMF, Zelt) was also selected as electrode material, a very unique multi-metalized fabric. This fabric is a very thin, lightweight, durable shielding option with an EMI shielding effectiveness as high as 10 GHz.

The basic design was built using conductive foam/fabric as both the ground plane and the patch which were then mounted on two different dielectric substrates of (Kapton HN, (5 mill) 0.125 mm in thickness, dielectric constant $\varepsilon_r = 3.4$) and ($RO3003$, 0.13 mm in thickness, dielectric constant $\varepsilon_r = 3$). Two points have to be mentioned here first, as $RO3003$ has the copper cladding on both sides, the desired size was completely dipped in Ferric Chloride (etchant) for approximately one hour to remove all the copper

on both side of the laminate producing a Polytetrafluoroethylene dielectric substrate (PTFE).

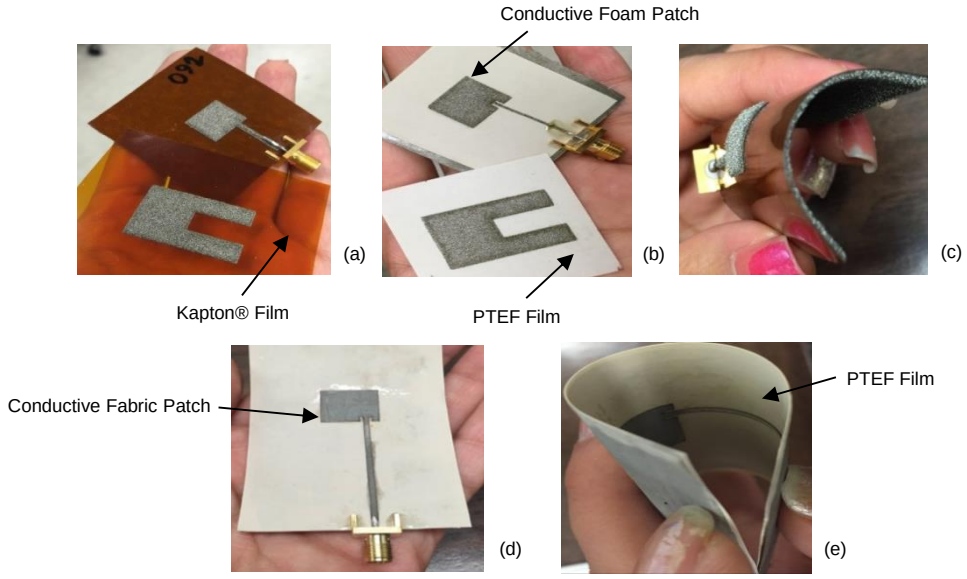

Figure 6-1 Implementing flexible sensor using conductive foam/fabric; (a) conductive foam antenna and reflector bonded on Kapton film; (b) conductive foam antenna and reflector bonded on PTFE film; (c) flexibility of antenna fabricated from conductive foam; (d) conductive fabric antenna; (e) flexibility of antenna fabricated from conductive fabric

Next, we tried to use the Kapton film with the same properties as the PTFE layer to avoid redesigning the patch antenna for new dielectric substrate properties. As well, we could now compare performance which would help prepare us for our next step. The antenna radiation patch, the ground plane, and the reflectors can be drawn on AUTOCAD and cut from conductive foam and fabric using laser machining at 100% speed and 70 % power and with a frequency of 2500 Hz (in vector setting). Using super glue, the patch antenna is assembled by bonding the ground plane to the substrate, followed by bonding the patch radiator to the substrate. As shown in Figure 6-1 (c) and

(e), the resulting patch antenna sensor is very flexible, can be easily bend and can conform to the residual limb.

To validate the performance of the antenna sensors, based on conductive foam and fabric, the transmission line of the patch antenna is connected to the SMA connectors. The scattering curve of the fabricated antennas sensors are obtained from VNA (Vector Network Analyzer) operating over the range of 5GHz-8GHz. Figure 6-2 shows that all fabricated antenna sensors, have a satisfactory resonant response, though all have different performance ratings.

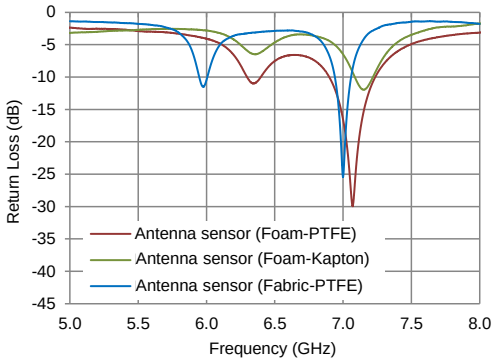

Figure 6-2 Comparison between the measured S_{11} curves of fabricated sensors; (conductive foam patch antenna based on Kapton substrate (Green-line); conductive foam patch antenna based on PTFE substrate (Red-line) and conductive fabric patch antenna based on PTFE substrate (Blue-line))

To prove the low performance of the fabricated conductive foam antenna sensor on Kapton substrate as compared with PTFE film, the experimental results obtained from this study can be compared with the same concept from previous studies. In [70, 71], the microstrip patch antennas for different dielectric constant materials were investigated, as well as the discrepancy between the fabricated conductive foam with Kapton and PTFE substrates. As the loss tangent and dielectric constant of Kapton ($\tan\delta \sim 0.001$, $\varepsilon_r = 3.4$)

are higher than the PTFE ($\tan\delta \sim 0.0002$, $\varepsilon_r = 3$), we could say that the efficiency and gain of the patch antenna will be decreased, which is realizable from Figure 6-1.

Although the conductive foam is more stretchable and tear and wrinkle resistant, from comparing the radiation characteristics of antenna sensors in Figure 6-2, we can observe that the efficiency and performance of a fabricated patch antenna based on fabric is better than the performance of the conductive foam. These results could be influenced by: (1) the conductivity of the electrode material; (2) the solderability of the electrode material

For the first hypothesis, it is clear that the choice of conductive material for the radiation element is one of the important criteria to assure good performance of the microstrip patch antenna. The conductivity of materials is inversely proportional to surface resistivity. Therefore, higher surface resistivity of conductive foam may decrease the efficiency of a fabricated conductive foam-based antenna. For the second hypothesis, as conductive foam is made from very fine metal, it is much harder to solder than fabrics and the connection is not robust enough which could be the cause for a slight mismatch between the measured frequencies.

6.2 Dielectric Substrate Material

Dielectric substrate is usually made of a thin sheet of low-loss insulating material like FR-4, Taconic TLC, Kapton and so on, which plays an important role in patch antenna performance. We observed that the base dielectric substrate of Rogers ($\mathrm{RO3003}$) laminate, which is the PTFE layer, has very low resistance to wear and tear. Therefore, we tried to use one kind of appropriate fabric which could be replaced with a PTFE layer resulting in improvement of the tear strength and resistance of the entire shear/pressure antenna sensor.

6.2.1 Mature Fabric Antenna Sensor

For fabricating the complete fabric-based sensor, conductive fabric is used for the radiating elements while non-conductive fabric is used as substrate. According to previously published work, different fabrics can be used instead of dielectric substrate. As there is a clear conception about the effect of thickness and dielectric constant of the substrate on antenna performance, the thin fabric with dielectric constant of around 2-3 was our choice. Commercially, textiles like Bondex can be attached with masking tape, and all we need is a hot iron to bond the conductive ground plane to one side of the fabric substrate. The top layout of the antenna is also transferred to the conductive fabric using a laser machine at 90 % speed and at 60 % power and with a frequency of 2500 Hz. Finally, the patch antenna is assembled by bonding the layout to the top of the substrate and ground plane using super glue (see Figure 6-3 (a)). Based on Figure 6-3 (b), the experimental results demonstrated that the fabricated antenna sensor has a satisfactory resonant response and a low loss. Since the same designed parameter for Rogers ($RO3003$) laminate was used for fabrication which has a different and higher dielectric constant compared to the fabric, the measured resonant frequencies of the fabric-based antenna sensor are higher than the simulated value which is 6.45 GHz for f_{01} and 7.6 GHz for f_{10}. The new design of for patch antennas - using fabric-based antenna sensors - and finding a suitable glue or epoxy for bonding fabrics, will be the next steps for future work.

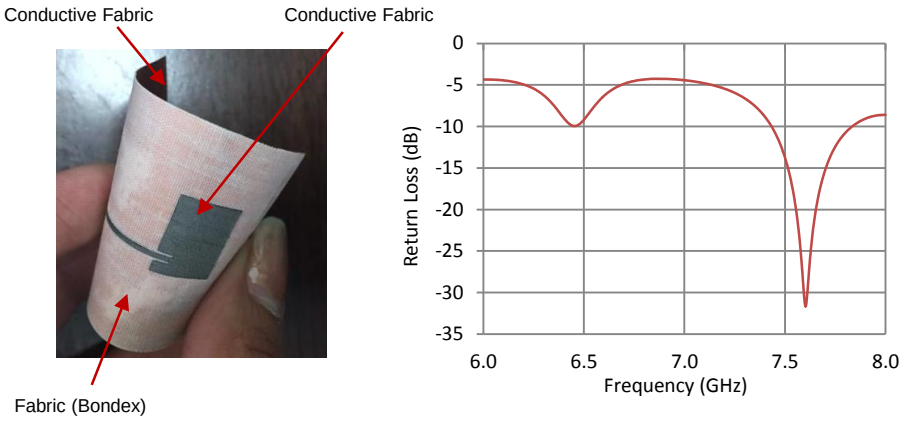

Figure 6-3 Complete fabric-based antenna sensor; (a) fabricated antenna sensor; (b) S_{11} parameter of the fabric-based antenna sensor

6.3 Meandering Transmission Line

There are only a few properties necessary to completely characterize the behavior of transmission lines for the patch antenna. Once realized, we will have the necessary information to design different transmission lines. The goal of this chapter is to enhance the performance of antenna sensors with a meandering transmission line. Meandering transmission lines are usually used in circuit designs as resistive elements (terminations), inductors, delay lines and phase shifters and can be used to reduce the size of the microstrip patch antenna which leads to minimizing cost. However, in this thesis, the objective of designing the microstrip patch antenna with meandering line is to ensure sufficient delay between the antenna feeding point and the SMA connector for data processing, and also to facilitate space division sensor multiplexing. Meandering transmission line is also more robust than a straight transmission line as it has greater stretchability. The design and fabrication of a patch antenna with a meandering transmission line is described step-by-step in this section.

6.3.1 Design and Simulation of Meandered line Patch Antenna

Antenna meandered transmission line is a set of horizontal and vertical lines which form a snaking patterns as they stream back and forth along their down-valley axis. The important design parameters for the meandered transmission line are the meandering length (i.e. the length of each element) and the meandering width (i.e. the separation between two consecutive elements) as shown in Figure 6-4 [72].

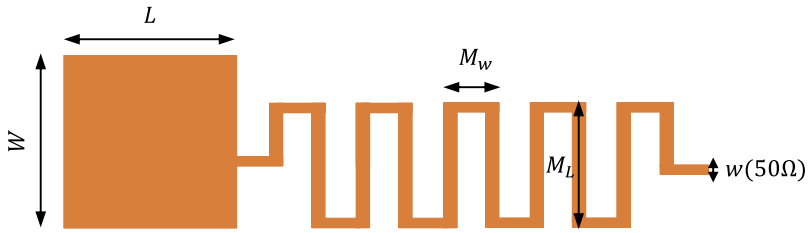

Figure 6-4 Patch antenna with meandering transmission line dimensions

For design of the meandered transmission line, the width and length of the transmission line can be calculated using the same procedures as in (Chapter 3; part 3.1). Also, the impedance of the transmission line is selected to match with the impedance of the antenna. Our ideal case with the use of transmission lines is that all waves travel at the same velocity and also arrive at the end of the transmission line at the same time. Therefore, the meandering length should be smaller than the quarter-wavelength of the center point of two frequencies and meandering width has to be more than twice the width of the transmission line. For finding the wavelength in the microstrip transmission line, first the free-space wavelength of the wave in the transmission line has to be calculated [73]. The wavelength of the line can then be calculated based on equation (5.4) in Chapter 5. The wavelength of the signal (center frequency between 6.1 and 6.85 GHz) in the transmission line is calculated (about 29.5 mm). Based on information provided in this part, the designed parameters are included: the width of the

transmission line is 0.35 mm; the length of the meandering line is 7 mm; and the width of the meandering line is 0.7 mm.

After calculating the dimensions of the transmission line, the bending type must then be considered. Three types of bend are used in the meandered transmission lines: square, curved and mitered. A curve bend is hard to fabricate and the meandered transmission line, with an abrupt stripline 90 bend, increases the amount of the capacitance to the transmission line which causes mismatching of the impedance and also an increase in the reflection. On the other hand, according to previous work, when the signal travels through the mitered bend type, the signal is less distorted and the reflection reduced, as compared with the square and curved bend type. In accordance with those test results, the mitered bend type was selected for the transmission line design. Three different methods are available for obtaining the mitered bend dimensions, which are discussed in the next sections.

- Regular Mitered Corner

This is the simplest way to compare the two other methods. As shown in Figure 6-5 (a), the corner has a $45°$ angle.

- Improved Mitered Corner

Figure 6-5 (b) shows another method which could mostly decrease the reflection of signals around the corner of meandered transmission line.

- Large Mitered Corner

The mitered bend dimensions as given in equation (6.1), (6.2) and (6.3), are a function of the width of transmission line and the height of substrate.

$$S = w\sqrt{2} \tag{6.1}$$

$$X = w\sqrt{2} \times (0.52 + 0.65e^{\left(-1.35\frac{w}{h}\right)}) \tag{6.2}$$

$$C = X\sqrt{2} - W \tag{6.3}$$

where w is the width of transmission line, h is the height of substrate.

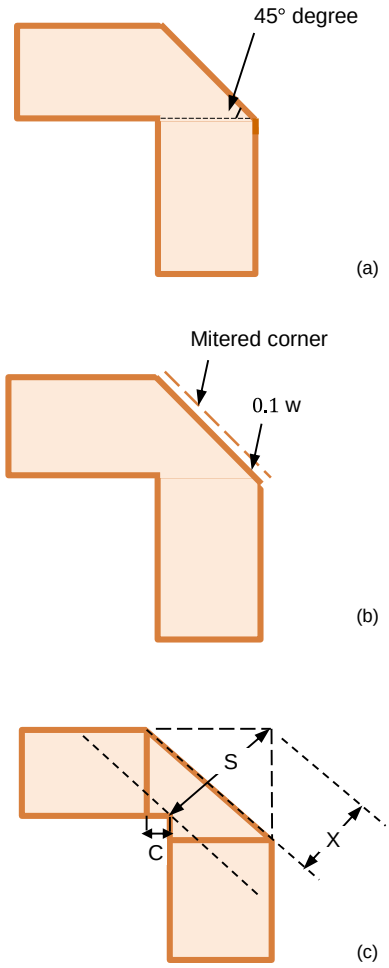

Figure 6-5 Three different configurations for mitered corners; (a) regular mitered corner; (b) improved mitered corner; (c) large mitered corner

The width of meandering line is similar to what we have calculated for the 50 Ω transmission line. As the width of transmission line narrows, there is not much variation in the dimensions of the mitered bend. Therefore, the first method is used, because it is simpler and exhibits better performance at higher frequencies and higher reflections.

Based on design parameters, a numerical simulation model was developed using an EM simulation tool, Sonnet pro, as shown in Figure 6-6 (a). Also, the radiation characteristics of the simulated mitered patch antenna are shown in Figure 6-6 (b).

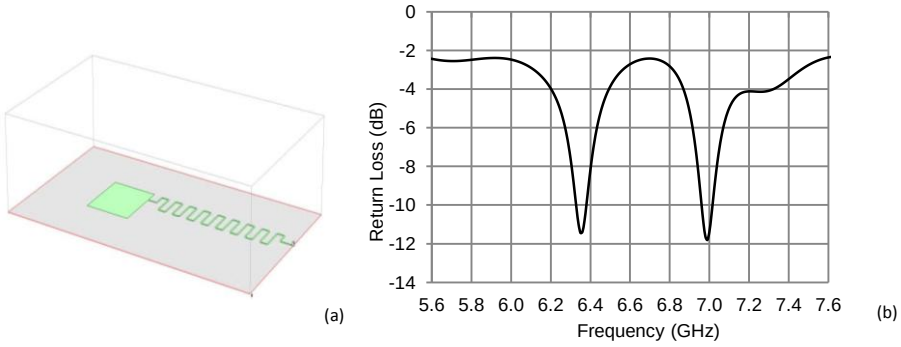

Figure 6-6 Antenna sensors with meandering transmission lines; (a) numerical simulation model of patch antenna with meandering transmission lines ;(b) Simulated radiation characteristics of proposed meandering antenna

6.3.2 Validation of Meandered Line Patch Antenna

The patch antenna, using meandered transmission lines, is fabricated with two different bending types, as shown in Figure 6-7. The meandering patch antenna fabricated with square corners did not have satisfactory resonant response. Experiments have proven that the signal is less distorted when traveling through the mitered bend type, as compared with the square corner bend type. As such, the mitered bend type with the slope edge of 45 degrees was selected for the transmission lines redesign. The photo-etched technique was again used for fabrication of the meandered transmission line antenna.

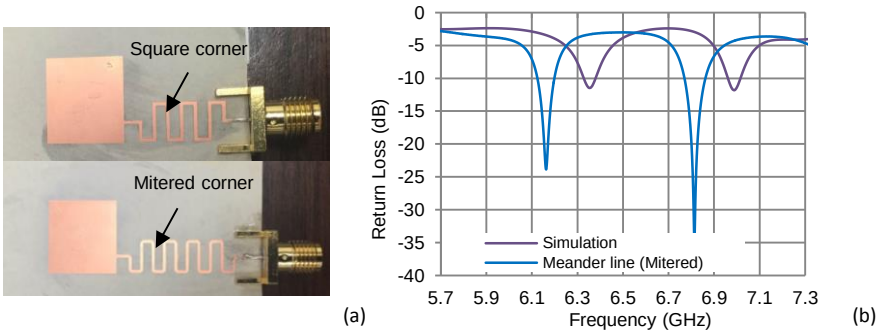

Figure 6-7 Meandered line patch antenna; (a) fabricated patch antennas with meandering transmission lines having two different bending types; (b) comparison between the measured and simulated S_{11} parameters of an antenna sensor with a mitered meandering transmission line

As shown in Figure 6-7, the numerical simulations of a designed meandered patch antenna produced a good account of what to expect when measuring the radiation characteristics of fabricated meandered patch antennas. As the number of turns increases, efficiency increases. Therefore, increasing the number of turns would be our group objective in the next step for future.

Chapter 7

CONCLUSION

In the present thesis, the prosthetic liner, with acceptable shear/pressure antenna sensors, are fabricated and able to be worn by an able-bodied volunteer. Different fabrication techniques are stablished to either integrate shear/pressure antenna sensors with commercial prosthetic liners, or to embed shear/pressure antenna sensors in custom-made prosthetic liners. In the former case, most of the attempt were either not usable or incompatible as prosthetic liners. Some of those rejected included the vacuum lamination technique and also the use of different adhesive materials for bonding technique. In the latter case, the characterization of the silicone material- which is considered to be the same as WillowWood commercial prosthetic liners- is given primary emphasis. After comparing and characterizing different elastic materials, PK16 RTV (see Appendix A.3) silicone material from Wacker Company was selected as the appropriate material for the custom-made prosthetic liners.

According to previously published work, a flexible, light weight and low cost shear/ pressure antenna sensors were re-designed for the thinnest Rogers laminate which is also more compatible with human skin. Unlike the previous group works, in this thesis, there was a challenge of existing the prosthetic liner material as the superstrate layer on top of the antenna sensor. The antenna sensor with prosthetic liner as superstrate was designed using conformal mapping technique, simulated using Sonnet Pro software and fabricated on flexible substrates. The radiation characteristics of microstrip patch antennas, with and without liner material, were validated by comparing the experimental measurements and their simulation results which was satisfactory. The results obtained showed that the resonant frequencies of the proposed patch antenna,

with existing superstrate, will shift to the left side and the values of return loss will decrease.

A method to design and then fabricate antenna sensors with long transmission lines was developed which enabled us to embed the antenna sensors in arbitrary locations of the real-size prosthetic liner. In addition, we identified that the long transmission line produced interference fringes in the S_{11} parameter of the antenna sensor, which could be removed by digital signal processing algorithms.

Two long antenna sensors were embedded in real size custom-made prosthetic liners, using two different fabrication techniques, for testing on an able-bodied volunteer. Unfortunately, we may not have time to characterize the antenna sensors' performance in real-size prosthetic liner material, but future research will provide that information.

Last but not least, our research proposed some novel improvement for antenna sensors such as like changing the electrode materials to conductive foam/fabric , as well as changing the substrate material to a common Bondex fabric. This research led us to the mature fabric antenna sensor. The comparison of the measured radiation characteristics of fabricated fabric sensors shows that they can replace the conventional antenna sensors with more flexibility, and with greater compatibility when in contact with human skin. In addition, the design of transmission lines for the microstrip patch antenna was improved by using meandering line. The use of meandering line led to sufficient delay between the antenna feeding point and the SMA connector for data processing of patch antenna arrays in the future.

Chapter 8

FUTURE WORKS

Future research with the fabricated prosthetic liner presented in this thesis should include testing and characterizing of antenna sensors performance when it is embedded in custom-made prosthetic liner. Actually, for the first step to verify the performance of antenna sensors, the final fabricated custom-made liner with two embedded antenna sensors worn by a volunteer and then covered with a wearable Patellar Tendon-Bearing Ankle Foot orthotic (PTB-AFO) device which is designed for able-bodied, as shown in Figure 8-1. The resonant frequencies of the antenna sensors could be measured using a vector network analyzer (VNA) which is connected to the antenna sensors via the SMA connector and data were collected at different fitness of the socket, e.g. very loose, loose, tight, and very tight. As shown in Figure 8-2, small frequency changes were observed from the sensor data. But in the future, a calibration procedure will be developed to correlate the frequency shifts to the pressure and shear stresses experienced by the limb. The collected data were processed to inversely determine the shear and pressure loads to evaluate the performance of the antenna sensor embedded in soft materials.

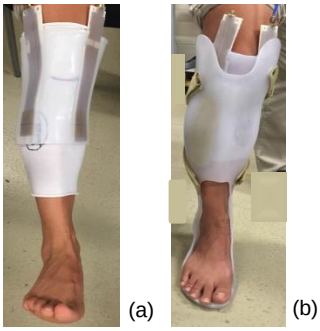

Figure 8-1 Final prototype of fabricated liner with antenna sensors; (a) the liner wore by a volunteer; (b) the liner inside a socket wore by a volunteer.

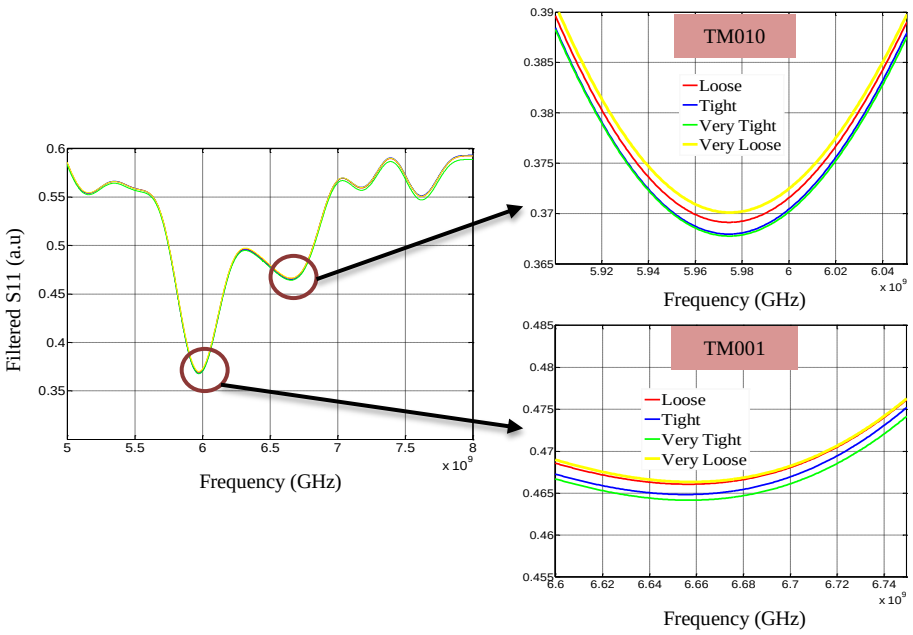

Figure 8-2 S11 parameter collected from the sensor embedded in the custom-made liner at different fitness of the socket

Embedding the proposed mature fabric antenna sensors in the real-size prosthetic liner needs to be further studied. Once the fabricated fabric sensors is embedded and worn by a volunteer for testing, we will have a better indication of what types of antenna sensors (Flexible Laminate or Fabrics based) can be used in future for initial clinic testing.

As the antenna sensors are very small sized and can be multiplexed to form a wireless sensing network, in the future, it will be novel to design an expandable matrix array of n^2 sensing sites $(n \times n)$ patch antenna sensors and embed in to the prosthetic liner which could be enable to measure shear and pressure interference stresses over a larger sensitive area and provide higher resolution than other reported sensors.

Appendix A

Material Data Sheet

A.1 Kapton Data Sheet

Table 1
Physical Properties of DuPont™ Kapton® HN at 23°C (73°F)

Property	Unit	1 mil 25µm	2 mil 50µm	3 mil 75µm	5 mil 125µm	Test Method
Ultimate Tensile Strength at 23°C, (73°F) at 200°C (392°F)	psi (MPa)	33,500(231) 20,000(139)	33,500(231) 20,000(139)	33,500(231) 20,000(139)	33,500(231) 20,000(139)	ASTM D-882-91, Method A*
Ultimate Elongation at 23°C, (73°F) at 200°C (392°F)	%	72 83	82 83	82 83	82 83	ASTM D-882-91, Method A
Tensile Modulus at 23°C, (73°F) at 200°C (392°F)	psi (GPa)	370,000 (2.5) 290,000 (2.0)	370,000 (2.5) 290,000 (2.0)	370,000 (2.5) 290,000 (2.0)	370,000 (2.5) 290,000 (2.0)	ASTM D-882-91, Method A
Density	g/cc	1.42	1.42	1.42	1.42	ASTM D-1505-90
MIT Folding Endurance	cycles	285,000	55,000	6,000	5,000	ASTM D-2176-89
Tear Strength-propagating (Elmendorf), N (lbf)		0.07 (0.02)	0.21 (0.02)	0.38 (0.02)	0.58 (0.02)	ASTM D-1922-89
Tear Strength, Initial (Graves), N (lbf)		7.2 (1.6)	16.3 (1.6)	26.3 (1.6)	46.9 (1.6)	ASTM D-1004-90
Yield Point at 3% at 23°C, (73°F) at 200°C (392°F)	MPa (psi)	69 (10,000) 41 (6,000)	69 (10,000) 41 (6,000)	69 (10,000) 41 (6,000)	69 (10,000) 41 (6,000)	ASTM D-882-91
Stress to produce 5% elong. at 23°C, (73°F) at 200°C (392°F)	MPa (psi)	90 (13,000) 61 (9,000)	90 (13,000) 61 (9,000)	90 (13,000) 61 (9,000)	90 (13,000) 61 (9,000)	ASTM D-882-92
Impact Strength at 23°C, (73°F)	N•cm•(ft lb)	78 (0.58)	78 (0.58)	78 (0.58)	78 (0.58)	DuPont Pneumatic Impact Test
Coefficient of Friction, kinetic (film-to-film)		0.48	0.48	0.48	0.48	ASTM D-1894-90
Coefficient of Friction, static (film-to-film)		0.63	0.63	0.63	0.63	ASTM D-1894-90
Refractive Index (sodium D line)		1.70	1.70	1.70	1.70	ASTM D-542-90
Poisson's Ratio		0.34	0.34	0.34	0.34	Avg. three samples, elongated at 5, 7, 10%
Low temperature flex life		pass	pass	pass	pass	IPC-TM-650, Method 2.6.18

*Specimen size 25 x 150 mm (1.6 in); jaw separation 100 mm (4 in), jaw speed, 50mm/min (2 in/min). Ultimate refers to the tensile strength and elongation measured at break.

A.2 Rogers (RO3003) Laminate Data Sheet

ROGERS CORPORATION

Data Sheet

Property	Typical Value[1]				Direction	Unit	Condition	Test Method
	RO3003	RO3035	RO3006	RO3010				
Dielectric Constant, ε_r Process	3.00 ± 0.04	3.50 ± 0.05	6.15 ± 0.15	10.2 ± 0.30	Z	-	10 GHz 23°C	IPC-TM-650 2.5.5.5 Clamped Stripline
[2] Dielectric Constant, ε_r Design	3.00	3.60	6.50	11.20	Z	-	8 GHz - 40 GHz	Differential Phase Length Method
Dissipation Factor, tan δ	0.0010	0.0015	0.0020	0.0022	Z	-	10 GHz 23°C	IPC-TM-650 2.5.5.5
Thermal Coefficient of ε_r	-3	-45	-262	-395	Z	ppm/°C	10 GHz -50 to 150°C	IPC-TM-650 2.5.5.5
Dimensional Stability	-0.06 0.07	-0.11 0.11	-0.27 -0.15	-0.35 -0.31	X Y	mm/m	COND A	IPC TM-650 2.2.4
Volume Resistivity	10^7	10^7	10^5	10^5		MΩ•cm	COND A	IPC 2.5.17.1
Surface Resistivity	10^7	10^7	10^5	10^5		MΩ	COND A	IPC 2.5.17.1
Tensile Modulus	900	1015	2068	1500	X, Y	MPa	23°C	ASTM D638
Moisture Absorption	0.04	0.04	0.02	0.05	-	%	D48/50	IPC-TM-650 2.6.2.1
Specific Heat	0.9		0.86	0.8		J/g/K		Calculated
Thermal Conductivity	0.50	0.50	0.79	0.95	-	W/m/K	50°C	ASTM D5470
Coefficient of Thermal Expansion	17 16 25	17 17 24	17 17 24	13 11 16	X Y Z	ppm/°C	-55 to 288°C	ASTM D3386-94
Td	500	500	500	500		°C TGA		ASTM D3850
Density	2.1	2.1	2.6	2.8		gm/cm³	23°C	ASTM D792
Copper Peel Strength	12.7	10.2	7.1	9.4		lb/in	1 oz. EDC After Solder Float	IPC-TM-2.4.8
Flammability	V-0	V-0	V-0	V-0				UL 94
Lead Free Process Compatible	YES	YES	YES	YES				

A.3 RTV Silicone Data Sheet

WACKER

ELASTOSIL® RTV-2 Silicone Rubber Grades for Prosthetics

	Blending ratio	Viscosity Component A	Viscosity Component B	Final hardness Shore A ISO 868	Final hardness Shore 00 TM 2240	Tensile strength ISO 37	Elongation at break ISO 37	Tear resistance ASTM D 624 B
Designation	A : B	[mPa·s]	[mPa·s]			[N/mm²]	[%]	[N/mm]
ELASTOSIL® P 7600	1:1	4,000	2,000	< 0	28	1.2	650	3
ELASTOSIL® P 7670	1:1	1,200	1,400	7	55	1.9	580	3
ELASTOSIL® P 7671	1:1	1,500	1,800	< 0	21	0.5	400	2
ELASTOSIL® P 7676	1:1	1,300	900	< 0	15	0.8	700	2
ELASTOSIL® P 7683/25	1:1	1,200	3,500	< 0	25	1.5	650	5
ELASTOSIL® P 7683/47	1:1	1,700	1,500	7	47	2.6	450	8
ELASTOSIL® P 7684/40	1:1	1,500	2,300	< 0	40	2.2	670	8
ELASTOSIL® P 7684/60	1:1	1,400	2,600	12	60	3.8	650	13
ELASTOSIL® PK 16	1:1	1,700	2,700	< 0	20	1.2	850	4

These figures are intended as a guide and should not be used in preparing specifications.

BLUESTAR SILICONES

Silbione® Soft Silicones for Orthotics and Prosthetics

Product	Mix Ratio (A:B)	Durometer (ShA)	Mixed Viscosity (cps)	Pot life (min.)	Tensile psi (N/mm2)	Elongation (%)	Tear ppi (kN/m)	Appearance
Silbione® RTVs								
RTV 4511 A/B	1:1	11 Sh00	1200	60	-	-	-	Translucent
RTV 4528 A/B	1:1	28 Sh00	4000	70	215 (1.5)	800	11 (2)	Translucent
RTV 4545 A/B	1:1	45 Sh00	1900	30	450 (2.9)	800	50 (9)	Translucent
RTV 4410 A/B	1:1	10	1650	60	430 (2.9)	800	80 (14)	Translucent
RTV 4410 QC A/B	1:1	10	2500	10	400 (2.7)	700	80 (14)	Translucent
RTV 4420 A/B	1:1	20	4000	60	580 (4.0)	550	85 (15)	Translucent
RTV 4420 QC A/B	1:1	20	7000	3	508 (3.5)	500	85 (15)	Translucent
RTV 4040	10:1	40	40000	120	920 (6.3)	340	120 (21)	Translucent
w/ cata 4020HT	10:1	22	40000	90	775 (5.3)	525	130 (23)	Translucent
w/ cata 4038	10:1	36	40000	120	900 (6.2)	340	100 (17)	Translucent
w/ cata 4045	10:1	45	40000	120	915 (6.2)	205	130 (23)	Translucent
Flesh Like Additive for RTVs								
Product	Appearance	Specific Gravity	Viscosity (cps)	Durometer (Sh00) added to RTV 4545 A/B				
FLESH 10 ADD	colorless to light straw	0.97	2200	20 parts Flesh Add	40 parts Flesh Add	50 parts Flesh Add	60 parts Flesh Add	70 parts Flesh Add
				47	26	18	8	5

A.4 Conductive Foam

waveseal
A 3GMETALWORX SOLUTION

Sheet Stock

Sheet Thickness	(250x250)	(500x500)	(500x1000)	(1000x1000)
.040 (1.0)	WS-4110-01-A	WS-4210-02-A	WS-4310-03-A	WS-4410-04-A
.060 (1.5)	WS-4115-01-A	WS-4215-02-A	WS-4315-03-A	WS-4415-04-A
.080 (2.0)	WS-4120-01-A	WS-4220-02-A	WS-4320-03-A	WS-4420-04-A
.100 (2.5)	WS-4125-01-A	WS-4225-02-A	WS-4325-03-A	WS-4425-04-A
.120 (3.0)	WS-4130-01-A	WS-4230-02-A	WS-4330-03-A	WS-4430-04-A
.140 (3.5)	WS-4135-01-A	WS-4235-02-A	WS-4335-03-A	WS-4435-04-A

Properties

- Shielding Effectiveness: 75dB (min) 10MHz - 10GHz
- Z-Resistivity: < .2 Ω/sq.
- Temp Range: -40°F to 200°F
- Avg. Compression: 2PSI @ 30%
- RoHS & REACH Compliant

Features

- High Shielding Performance
- Very Low Compression Force
- Cuts Easily into Intricate Shapes
- Standard with Conductive PSA
- Easy to Peel and Stick

Applications

- I/O Panels
- Connector Gaskets
- Backplanes
- Access Panels
- Door Seams
- PCB Shielding

A.5 Adhesive Materials

Sil-Poxy®

Silicone Rubber Adhesive

TECHNICAL OVERVIEW

Mixed Viscosity, Thick-paste

Specific Gravity, g/cc: 1.12

Working Time: 5 minutes (73°F/23°C)

Cure time: 12 minutes (73°F/23°C)

Color: Translucent

Shore A Hardness: 40

Tensile Strength, psi: 750

Elongation @ Break: 750%

Tear Strength: 100 ppi

Peel Strength: 100 ppi

Temperature Range: -50°F (-41°C) to 500°F (260°C)

Note: Tests done bonding silicone to silicone
* All values measured after 7 days at 73°F/23°C

System 2000 Epoxy Resin

	2000	2020	2060	2120	ASTM Method
Color	Lt. Amber	Amber	Amber	Amber	Visual
Viscosity, @ 77° F, centipoise	1,650 cps	150-175 cps	190-200 cps	200-250 cps	D2393
Specific Gravity, gms./cc	1.15	0.96	0.96	0.95	D1475
Mix Ratio, By Wt		100 : 23 By Weight, or 4 to 1 By Volume	100 : 27 By Weight, or 3 to 1 By Volume		D2471
Pot Life, 4 fl. Oz. Mass @ 77° F		20 minutes	1 hour	2 hour	PTM&W

LOCTITE

Technical Data Sheet

LOCTITE® SF 7701™

Known as LOCTITE® 7701™
January 2015

PRODUCT DESCRIPTION

LOCTITE® SF 7701™ provides the following product characteristics:

Technology	Primer - Cyanoacrylate
Chemical Type	Aliphatic amine
Solvent	n-Heptane
Active Ingredient Concentration, %	0.08 to 0.12[LMS]
Appearance	Clear colorless liquid[LMS]
Fluorescence	Positive under UV light[LMS]
Viscosity	Very low
Cure	Not applicable
Application	CA surface primer

LOCTITE® SF 7701™ is used to make polyolefin and other low energy surfaces suitable for bonding with Loctite cyanoacrylate adhesives. On such treated surfaces the cured performance of LOCTITE® cyanoacrylate adhesives is generally similar to that described in the TDS for the relevant adhesive. It is only recommended for difficult to bond substrates which include polyethylene, polypropylene, polytetrafluoroethylene (PTFE) and thermoplastic rubber materials. It is not recommended in assemblies where high peel strength is required. LOCTITE® SF 7701™ is suitable for use in the assembly of disposable medical devices.

ISO-10993

An ISO 10993 Test Protocol is an integral part of the Quality Program for LOCTITE® SF 7701™. LOCTITE® SF 7701™ has been qualified, in conjunction with LOCTITE® 4014, to Loctite's ISO 10993 Protocol as a means to assist in the selection of products for use in the medical device industry. Certificates of Compliance are available at www.loctite.com or through the Henkel Loctite Quality Department.

TYPICAL PROPERTIES

Specific Gravity @ 25 °C	0.68
Viscosity @ 20 °C, mPa·s (cP)	1.25
Drying Time @ 20 °C, seconds	≤30
On Part Life, hours	≤8

Flash Point - See SDS

TYPICAL PERFORMANCE

Fixture time and cure speed achieved as a result of using LOCTITE® SF 7701™ depend on the adhesive used and the substrate bonded.

Effect on Cure Speed of Cyanoacrylate Adhesives

LOCTITE® SF 7701™ also behaves as an activator and accelerates the cure speed of cyanoacrylate adhesives. Fixturing time on most primed substrates is less than 5 seconds but 24 hours at room temperature (22 °C) should be allowed for adhesive to develop maximum bond strength.

Effect on Cured Properties of Cyanoacrylate Adhesives

Products 406, 496 and 460 are based on ethyl, methyl and ß-Methoxyethyl esters respectively. Other LOCTITE® liquid products based on these esters will behave in a similar fashion to these examples. LOCTITE® SF 7701™ is not recommended for use with gel products.

TYPICAL PERFORMANCE OF CURED MATERIAL

Performance Data

Substrates treated with LOCTITE® SF 7701™
After 24 hours @ 22 °C / 55% RH:
Lap Shear Strength, ISO 4587:

Polypropylene and LOCTITE® 406™	N/mm² (psi)	3 to 10 (440 to 1,450)
Polypropylene and LOCTITE® 496™	N/mm² (psi)	2 to 7 (290 to 1,015)
Polypropylene and LOCTITE® 460™	N/mm² (psi)	1 to 4 (145 to 580)
Thermoplastic Rubber and LOCTITE® 406™	N/mm² (psi)	2 to 6 (290 to 870)
Polytetrafluorethylene (PTFE) and LOCTITE® 406™	N/mm² (psi)	1 to 6 (145 to 870)
HDPE treated with LOCTITE® SF 7701™ to:		
Mild steel (grit blasted) without primer and LOCTITE® 406™	N/mm² (psi)	4 to 10 (580 to 1,450)
Polypropylene treated with primer and LOCTITE® 496™	N/mm² (psi)	5 to 15 (725 to 2,175)

Appendix B

SolidWorks Layout

B.1 Prosthetic Liner Mold

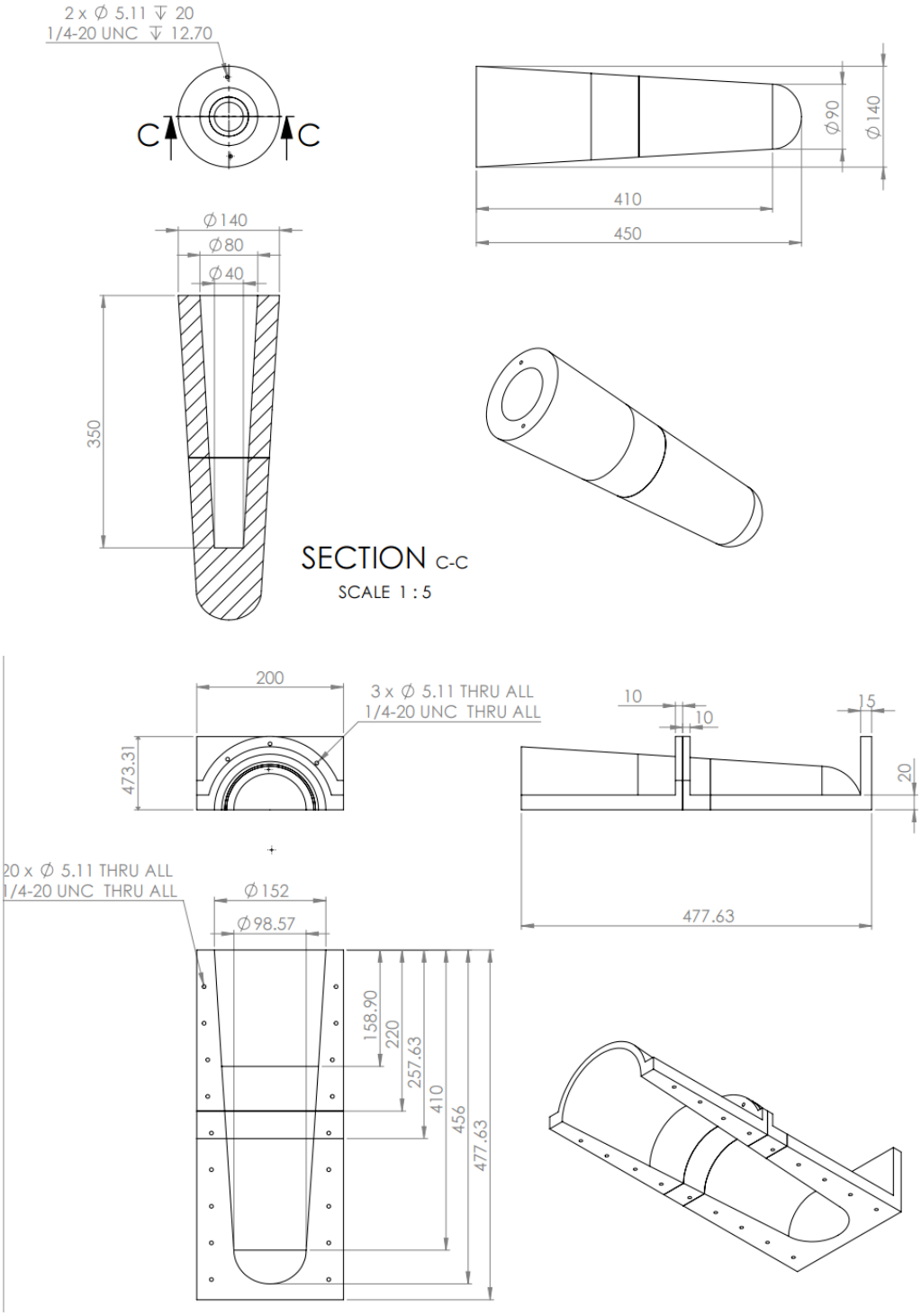

B.2 SMA Supporter

(a) Bottom Part

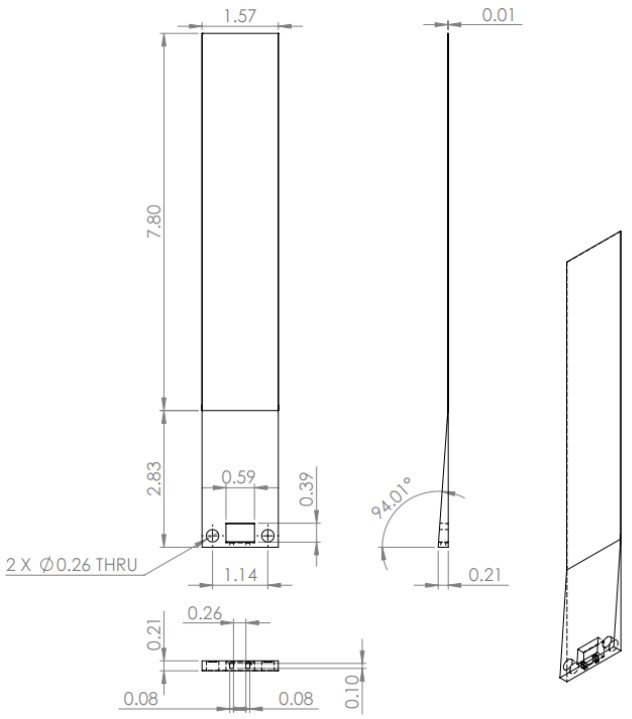

(b) Top Part

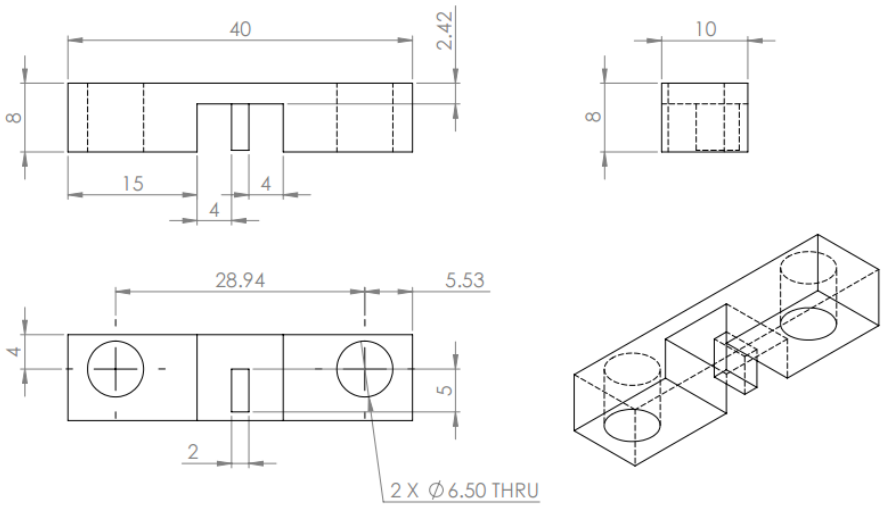

References

[1] S. Laing, P. V. Lee and J. C. Goh. Engineering a trans-tibial prosthetic socket for the lower limb amputee. Annals of the Academy of Medicine-Singapore 40(5), pp. 252. 2011.

[2] D. T. Mitchell and S. L. Snyder. Narrative Prosthesis: Disability and the Dependencies of Discourse 2000.

[3] K. Norton. A brief history of prosthetics. Motion Magazine 172007.

[4] J. Finch. The ancient origins of prosthetic medicine. Lancet 377(9765), pp. 548-549. 2011.

[5] O. Fliegel and S. Feuer. Historical development of lower-extremity prostheses. Arch. Phys. Med. Rehabil. 47(5), pp. 275-285. 1966.

[6] J. R. Kirkup. A History of Limb Amputation 2007.

[7] K. C. Norris. Rehabilitation process of lower extremity amputees. 2000.

[8] D. Serlin. Artificial Parts, Practical Lives: Modern Histories of Prosthetics 2002.

[9] A. J. Thurston. Paré and prosthetics: The early history of artificial limbs. ANZ J. Surg. 77(12), pp. 1114-1119. 2007.

[10] M. S. Kocher. Early limb salvage: Open tibia fractures of ambroise paré (1510–1590) and percivall pott (1714–1789). World J. Surg. 21(1), pp. 116-122. 1997.

[11] R. Ham and L. T. Cotton. Limb Amputation: From Aetiology to Rehabilitation 2013.

[12] C. A. Caspers, "Hypobarically-controlled socket for artificial limb ,", 2003.

[13] C. A. Caspers, "Pulsating pressure chamber and method for fluid management ,", 2011.

[14] M. B. Silver-Thorn, J. W. Steege and D. S. Childress. A review of prosthetic interface stress investigations. Journal of Rehabilitation Research and Development 33(3), pp. 253. 1996.

[15] J. T. Peery, W. R. Ledoux and G. K. Klute. Residual-limb skin temperature in transtibial sockets. Journal of Rehabilitation Research and Development 42(2), pp. 147. 2005.

[16] D. H. Bautista. Electromagnetic Suspension System for Prosthetic Limbs that Compensates for Residual Limb Shrinkage 2014.

[17] J. E. Sanders and S. Fatone. Residual limb volume change: Systematic review of measurement and management. J. Rehabil. Res. Dev. 48(8), pp. 949-986. 2011.

[18] J. E. Sanders, D. S. Harrison, K. J. Allyn and T. R. Myers. Clinical utility of in-socket residual limb volume change measurement: Case study results. Prosthet. Orthot. Int. 33(4), pp. 378-390. 2009.

[19] K. Case, M. Porter, D. Gyi, R. Marshall and R. Oliver. Virtual fitting trials in 'design for all'. J. Mater. Process. Technol. 117(1), pp. 255-261. 2001.

[20] S. Ramakrishna, J. Mayer, E. Wintermantel and K. W. Leong. Biomedical applications of polymer-composite materials: A review. Composites Sci. Technol. 61(9), pp. 1189-1224. 2001.

[21] D. Murphy. Medical management of the residual limb. Fundamentals of Amputation Care and Prosthetics pp. 215. 2013.

[22] Y. Fung. Biomechanics: Mechanical Properties of Living Tissues 2013.

[23] A. F. Mak, M. Zhang and D. A. Boone. State-of-the-art research in lower-limb prosthetic biomechanics-socket interface: A review. Journal of Rehabilitation Research and Development 38(2), pp. 161. 2001.

[24] I. Mohammad and H. Huang. Shear sensing based on a microstrip patch antenna. Measurement Science and Technology 23(10), pp. 105705. 2012.

[25] S. Deshmukh, I. Mohammad, X. Xu and H. Huang. Unpowered antenna sensor for crack detection and measurement. Presented at SPIE Smart Structures and Materials Nondestructive Evaluation and Health Monitoring. 2010,

[26] F. Appoldt, L. Bennett and R. Contini. Stump-socket pressure in lower extremity prostheses. J. Biomech. 1(4), pp. 247-257. 1968.

[27] R. Williams, D. Porter, V. Roberts and J. Regan. Triaxial force transducer for investigating stresses at the stump/socket interface. Medical and Biological Engineering and Computing 30(1), pp. 89-96. 1992.

[28] E. A. Al-Fakih, N. A. Abu Osman and F. R. Mahmad Adikan. Techniques for interface stress measurements within prosthetic sockets of transtibial amputees: A review of the past 50 years of research. Sensors 16(7), pp. 1119. 2016.

[29] J. E. Sanders and C. H. Daly. Measurement of stresses in three orthogonal directions at the residual limb-prosthetic socket interface. IEEE Transactions on Rehabilitation Engineering 1(2), pp. 79-85. 1993.

[30] J. Goh, P. Lee and S. Chong. Stump/socket pressure profiles of the pressure cast prosthetic socket. Clin. Biomech. 18(3), pp. 237-243. 2003.

[31] K. Akca and M. C. Çehreli. A photoelastic and strain-gauge analysis of interface force transmission of internal-cone implants. Int. J. Periodontics Restorative Dent. 28(4), 2008.

[32] B. J. Hafner and J. E. Sanders. Considerations for development of sensing and monitoring tools to facilitate treatment and care of persons with lower-limb loss: A review. J. Rehabil. Res. Dev. 51(1), pp. 1-14. 2014. . DOI: 10.1682/JRRD.2013.01.0024 [doi].

[33] M. C. Hsieh, Y. K. Fang, M. Ju, G. Chen, J. Ho, C. Yang, P. M. Wu, G. Wu and T. Y. Chen. A contact-type piezoresistive micro-shear stress sensor for above-knee prosthesis application. J Microelectromech Syst 10(1), pp. 121-127. 2001.

[34] K. Sundara-Rajan, G. I. Rowe, A. Bestick, A. V. Mamishev, G. K. Klute and W. R. Ledoux. Capacitive sensing of interfacial forces in prosthesis. Presented at Proc. 2010 IEEE Int. Workshop on Medical Measurements and Applications Proceedings (MeMeA). 2010, .

[35] P. Laszczak, L. Jiang, D. L. Bader, D. Moser and S. Zahedi. Development and validation of a 3D-printed interfacial stress sensor for prosthetic applications. Med. Eng. Phys. 37(1), pp. 132-137. 2015.

[36] M. I. Tiwana, S. J. Redmond and N. H. Lovell. A review of tactile sensing technologies with applications in biomedical engineering. Sensors and Actuators A: Physical 179pp. 17-31. 2012.

[37] Y. Zhang, H. Ouyang, C. T. Lim, S. Ramakrishna and Z. Huang. Electrospinning of gelatin fibers and gelatin/PCL composite fibrous scaffolds. Journal of Biomedical Materials Research Part B: Applied Biomaterials 72(1), pp. 156-165. 2005.

[38] L. S. Lincoln, M. Quigley, B. Rohrer, C. Salisbury and J. Wheeler. An optical 3D force sensor for biomedical devices. Presented at 2012 4th IEEE RAS & EMBS International Conference on Biomedical Robotics and Biomechatronics (BioRob). 2012, .

[39] S. Zachariah and J. Sanders. Standing interface stresses as a predictor of walking interface stresses in the trans-tibial prosthesis. Prosthet. Orthot. Int. 25(1), pp. 34-40. 2001.

[40] J. Frieden, J. Cugnoni, J. Botsis, T. Gmür and D. Ćorić. High-speed internal strain measurements in composite structures under dynamic load using embedded FBG sensors. Composite Structures 92(8), pp. 1905-1912. 2010.

[41] G. M. Hefferman, F. Zhang, M. J. Nunnery and H. Huang. Integration of surface electromyographic sensors with the transfemoral amputee socket: A comparison of four differing configurations. Prosthet. Orthot. Int. 39(2), pp. 166-173. 2015. . DOI: 10.1177/0309364613516484 [doi].

[42] I. Mohammad and H. Huang. Pressure and shear sensing based on microstrip antennas. Presented at SPIE Smart Structures and Materials Nondestructive Evaluation and Health Monitoring. 2012, .

[43] Hao Jiang and Haiying Huang, "Simultaneous shear and pressure sensing based on patch antenna," in 2015, .

[44] T. C. Edwards, T. Edwards and M. Steer. Foundations for Microstrip Circuit Design 2016.

[45] P. Bhartia , Inder Bahl , R. Garg, and A. Ittipiboon, Ed., Microstrip Antenna Design Handbook. Norwood, MA: Artech House Inc. Norwood, 2001.

[46] B. Patel, T. Narang and S. Jain. Microstrip patch antenna-A historical perspective of the development. Presented at Conference on Advances in Communication and Control Systems. 2013, .

[47] S. Srivastava, A. Khandelwal and S. Sharma. Microstrip patch antenna: A survey. IOSR J.Electr.Electron.Eng 9(4), pp. 7-13. 2014.

[48] R. Patil and S. Popalghat. A review of various types of patch antenna.

[49] Alaa Ibrahim Abunjaileh, "Multimode and Multiband Microstrip Antennas," 2007.

[50] H. Elsadek. Microstrip Antennas for Mobile Wireless Communication Systems 2010.

[51] C. A. Balanis. Antenna Theory: Analysis and Design 2016.

[52] H. K. Varshney, M. Kumar, A. Jaiswal, R. Saxena and K. Jaiswal. A survey on different feeding techniques of rectangular microstrip patch antenna. International Journal of Current Engineering and Technology, Accepted 22014.

[53] Haiying Huang, Jun Yao, Shahnavaz Eilbeigi, "Simultaneous shear/pressure antenna sensor," in Corfu, Greece, 2016, .

[54] H. J. Haiying Huang, "Sensor assembly, method and device for monitoring shear force and pressure on a structure ,", 2015.

[55] P. Hazdra, M. Polivka and V. Sokol. Microwave antennas and circuits modeling using electromagnetic field simulator. Radioengineering 2005.

[56] yahya entiefa mansour, "Single Slot Dual Band Microstrip Antenna For Wimax Application," june 2014.

[57] S. D. Gupta and A. Singh. Design and analysis of multi dielectric layer microstrip antenna with varying superstrate layer characteristics. International Journal of Advances in Engineering& Technology 3pp. 55-68. 2012.

[58] Anonymous "Design of multidielectric layer microstrip antenna and superstrate effects," in Anonymous CHAPTER 3, pp. 77-119.

[59] J. Svacina. Analysis of multilayer microstrip lines by a conformal mapping method. IEEE Trans. Microwave Theory Tech. 40(4), pp. 769-772. 1992.

[60] H. A. Wheeler. Transmission-line properties of parallel strips separated by a dielectric sheet. IEEE Trans. Microwave Theory Tech. 13(2), pp. 172-185. 1965.

[61] Z. Ahmad. Polymeric dielectric materials. Dielectric Material pp. 3-26. 2012.

[62] M. Grilo and F. S. Correra. Parametric study of rectangular patch antenna using denim textile material. Presented at Microwave & Optoelectronics Conference (IMOC), 2013 SBMO/IEEE MTT-S International. 2013, .

[63] Gougeon Brothers, "Vacuum Bagging Techniques (WEST SYSTEM® Epoxy)," 2010.

[64] (). Vacuum Bagging Components.

[65] (). Vacuum Bagging Equipment and Techniques for Room-Temp Applications.

[66] (). Comparison of different prosthetic material.

[67] S. J. Covey and J. Muonio. Flow constraint and loading rate effects on prosthetic liner material and human tissue mechanical response. JPO: Journal of Prosthetics and Orthotics 12(1), pp. 15-32. 2000.

[68] C. Jeffrey Brinker, "Dip coating," in Chemical Solution Deposition of Functional Oxide Thin Films,Anonymous 2013, .

[69] J. R. Ojha and M. Peters. Patch Antennas and Microstrip Lines 2010.

[70] H. Wang, Z. Zhang, Y. Li and Z. Feng. A dual-resonant shorted patch antenna for wearable application in 430 MHz band. IEEE Transactions on Antennas and Propagation 61(12), pp. 6195-6200. 2013.

[71] R. Salvado, C. Loss, R. Gonçalves and P. Pinho. Textile materials for the design of wearable antennas: A survey. Sensors 12(11), pp. 15841-15857. 2012.

[72] S. Shrestha. Chipless RFID Sensor Tag System with Microstrip Transmissionline Based ID Generation Schemes 2009.

[73] J. Xu and R. Chen. Meandered microstrip transmission line based ID generation circuit for chipless RFID tag. Presented at Electrical Design of Advanced Packaging and Systems Symposium (EDAPS), 2011 IEEE. 2011, .

Biographical Information

Shahnavaz Eilbeigi was born in Isfahan, Iran, in July 1990. She completed her Bachelors Degree in Mechanical Engineering from the Shahrekord University, Iran, in 2014. She then joined the University of Texas at Arlington to pursue her Masters Degree in Mechanical Engineering. She worked for two years as a research assistant with Prof.Huang at the Advanced Sensor Technology Laboratory. During the course of her research, she worked on the area of antenna sensor design and fabrication and she successfully developed a smart sensing prosthetic liner and wearable antenna sensors.